Spring 2016

Material properties affecting the penetration of metal targets by copper linear shaped charges

Kevin Lee Phelps

MATERIAL PROPERTIES AFFECTING THE PENETRATION OF METAL

TARGETS BY COPPER LINEAR SHAPED CHARGES

By

KEVIN LEE PHELPS

A THESIS

Presented to the Faculty of the Graduate School of the

MISSOURI UNIVERSITY OF SCIENCE AND TECHNOLOGY

In Partial Fulfillment of the Requirements for the Degree

MASTER OF SCIENCE IN EXPLOSIVES ENGINEERING

2016

Approved by

Dr. Paul Worsey

Dr. Jason Baird

Dr. Catherine Johnson

www.manaraa.com

ABSTRACT

A linear shaped charge (LSC) is an explosive device used in demolition, aerospace, and in other applications that require the cutting of metal. Users of LSC's typically know the size of shaped charge needed to cut their target but commonly encounter previously untested materials. The motivation for this thesis is to provide an understanding as to what target material properties are good indicators of cutting performance so the selection of LSC can be more efficient. The author found that penetration theories for other types shaped charges were insufficient for the LSC, possibly because of the relatively slow projectile created by an LSC compared to that of, for example, a conical shaped charge (CSC). Penetration theories describing the performance of CSCs are inadequate for predicting LSC performance because of the differences in penetrator formation and velocity.

This report gauges the success and performance of LSC by the amount of penetration seen in the target. The material properties of targets that have the most effect on penetration were studied by firing LSCs into metal targets. Target materials and LSC sizes were chosen based on availability, input from industry, and the range of material properties they represented.

This report concludes that ultimate tensile strength of the target plays a greater role in resisting penetration by the copper projectile from an LSC than the target material's density or yield strength, which are influential components in early CSC penetration theories.

ACKNOWLEDGMENTS

The author would like to thank his advisor, Dr. Paul Worsey, for his support and insight into this project. The author would also like to thank his committee members, Dr. Jason Baird and Dr. Catherine Johnson, for their constant advice and guidance during the course of this research.

TABLE OF CONTENTS

LIST OF FIGURES

LIST OF TABLES

1. INTRODUCTION

The linear shaped charge (LSC) is a subset of a broad category of explosive devices that utilize specific geometry to achieve a desired effect upon detonation. The desired effect is typically explosively forming a projectile from a liner fitted to the device. Other types of shaped charges include the more frequently studied conical shaped charge (CSC) and the explosively formed penetrators (EFP). The LSC has not been studied as extensively as CSCs, and as a result, does not have penetration theories as robust as current CSC models.

The effort described in this master's thesis outlines a series of tests that were conducted to investigate the influence of target material properties on the performance of LSC penetration. Industry feedback shows that some applications involving cutting older steels resulted in decreased performance. Data gathered by the author prior to this thesis also indicates that certain material properties, such as the target's tensile strength, are strong indicators of an LSC's performance.

The motivation behind this series of experiments is to provide data to the manufacturer for distribution so the users of the shaped charges can make an informed decision when selecting a charge for a particular application. The manufacturer of the LSC provided targets and the charges for these experiments. Resource limitations restricted the author's ability to test iterations of each charge-target configuration. The result was a series of tests that comprised of five target materials with three LSC sizes. The author chose each target material with consideration for its prevalence in applications that typically use LSCs with input from the LSC manufacturer to achieve a range of material properties.

Users of LSCs often find that additional fracturing of a target will occur past the penetration depth (Smith). However, the scope of this report includes only the plastically

deformed portion of the penetration and not any additional brittle fracturing that may result. The analysis primarily focuses on the material properties of the target, such as yield strength, tensile strength, density, and elastic moduli, and their influences on the depth of penetration.

A number of predictive models exist for the penetration of shaped charges and projectiles into targets. The next section describes some of these models as well as their relevancy to LSC penetration.

2. LITERATURE REVIEW

This chapter reviews some past efforts and discussions on penetration theories on multiple types of projectiles. These projectiles include CSCs and long rod penetrators. This literature review will give the reader an idea of previous research conducted in this field and some background to what has motivated this thesis.

2.1. PYROTECHNIC SHOCK: A LITERATURE SURVEY OF THE LSC, (Smith)

This thesis uses some of the same material used in Smith's 1984 paper, sponsored by NASA that reviews LSCs. In addition to penetration, pyrotechnic and shock testing methods are reviewed. This section concentrates on the performance testing and comparisons between the aluminum and stainless steel used in his research.

In Smith's paper, Equation 1 describes the penetration of an LSC into a target based on the amount of explosives used, also called the core load. LSC manufacturers still use this equation today. For example, the manufacturer of the LSC used in this thesis uses a variation of this equation with an adjusted exponent of 0.5.

$$\frac{T_1}{T_2} = \left(\frac{W_1}{W_2}\right)^{0.6} \tag{1}$$

Where T1 is the unknown penetration on the charge whose core load is W1 and T2 and W2 is a known penetration and core load for a second known shaped charge. Using the same target material, the penetration of an LSC can be determined based on the core load and comparing it to an LSC with known penetration and core load. Figure 2.1 shows the performance of an LSC compared to the core load. The LSC mentioned in this research is flexible and uses a lead sheath. However, the reader can see that the aluminum targets

experiences almost twice as much penetration that the 304 stainless. Smith also states that

copper liners results in the most penetration compared to the amount of explosives used.
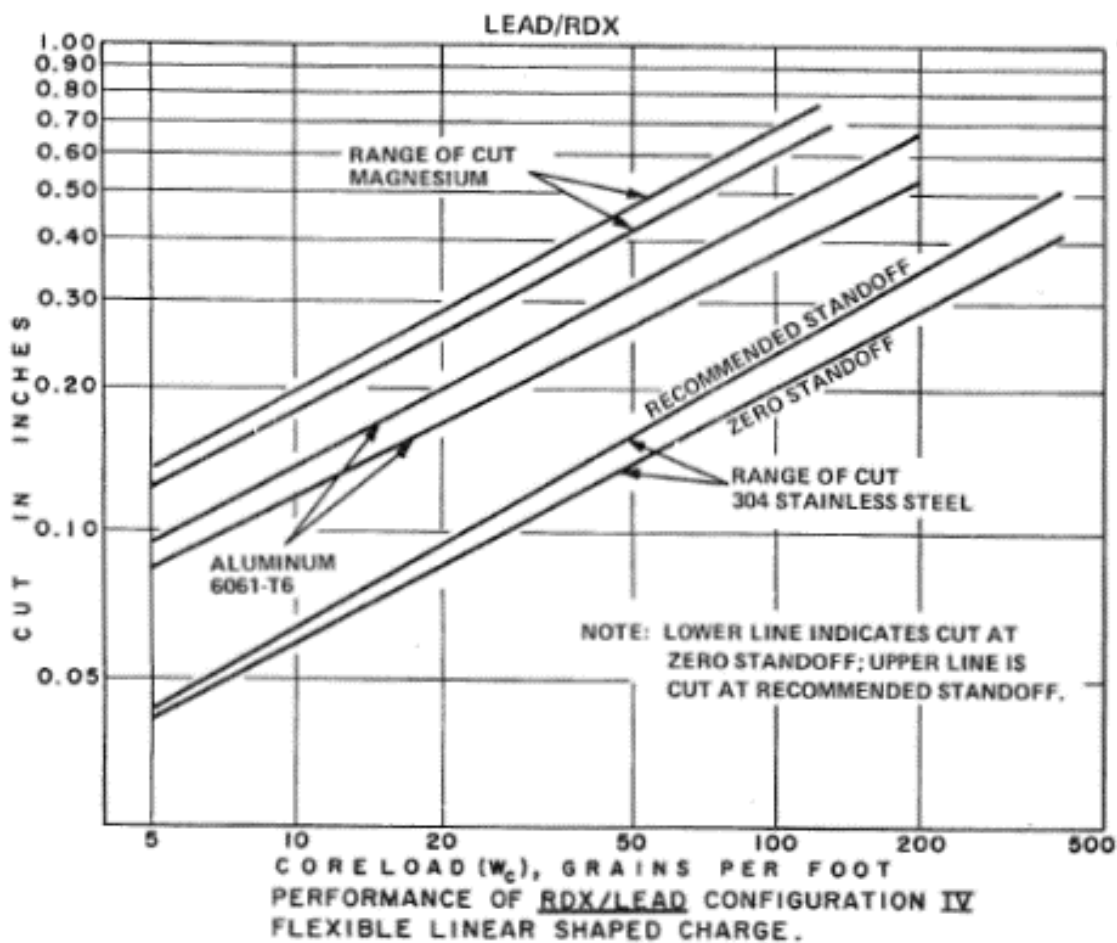
Figure 2.1. Chart showing LSC penetration into different materials using different core loads (Smith)

Figure 2.2 is another chart showing the total cut, which is the penetration of the

LSC plus the fracture, which Smith states can account for one-half of the total cut. The

shock-induced fracturing was not measured for this thesis and was not included when

describing the performance of the LSC.
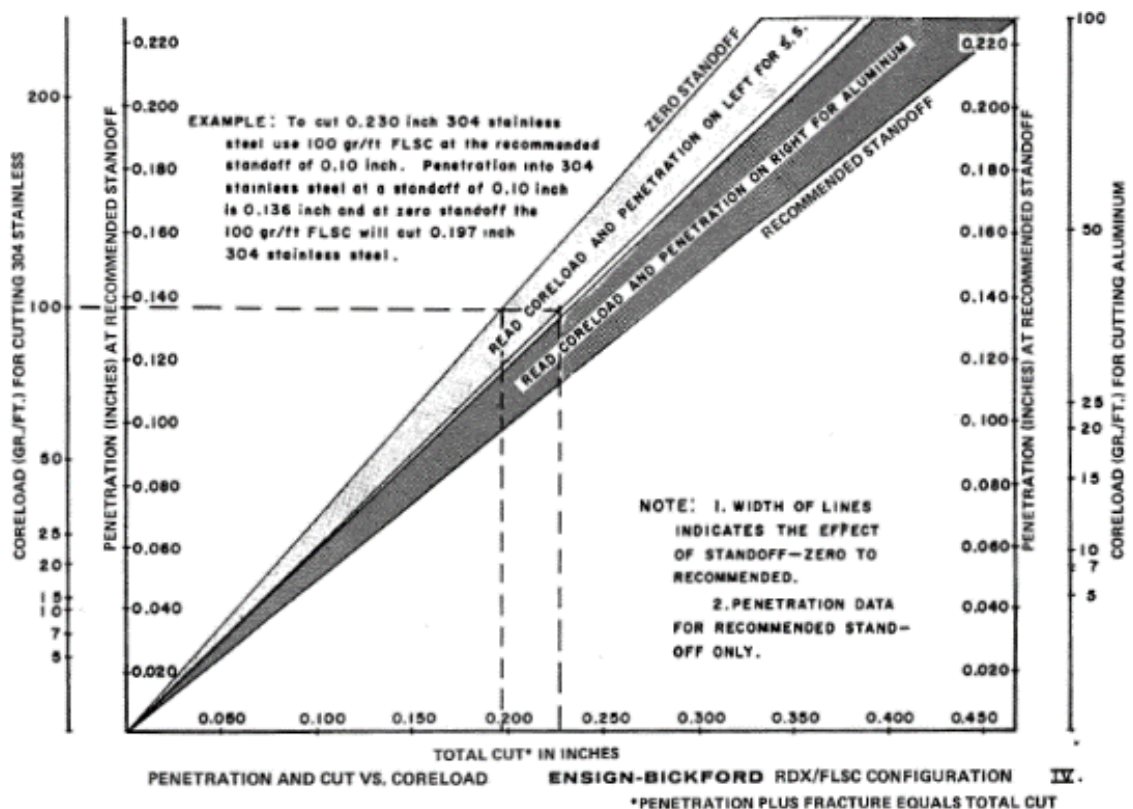
Figure 2.2. Total cut of LSC with Fracture added to the penetration (Smith)

2.2. ANNULAR PRECISION LINEAR SHAPED CHARGE, (Vigil and Marchi)

This research was conducted to create a system that would cut four-inch diameter holes in 304 stainless steel spherical tanks. Sandia National Laboratories developed the Precision Linear Shaped Charge (PLSC). Sandia used an LSC with a 65 grain per foot core load and recorded the penetration of the projectile into different targets. The LSC is built with a copper sheath and a 76-degree apex angle, which is similar to the charges used for this thesis (shown in Figure 2.3).Though this system was developed for cutting 304L stainless, 6061-T6 aluminum and 1018 steel were also used for testing. The maximum penetration into the steel and aluminum was 0.145 inches and 0.30 inches respectively.
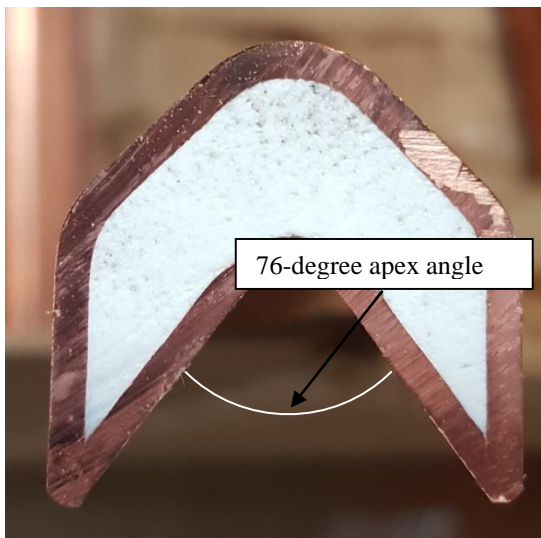
Figure 2.3. Cross section of a copper-sheathed LSC showing the apex angle

2.3. PENETRATION

The projectile formed by an LSC moves slower and is formed differently that the projectile from a CSC. An LSC projectile is slower and coherent while the jet from a CSC is much faster and tends to fragment because of velocity differences in the leading and trailing segments.

The author found that many of the available penetrations theories are focused on predicting the penetration of CSCs. A report discussing some of these theories noted that the jet resulting from a CSC has a velocity gradient throughout the length of the jet, which does not have a constant kinetic energy (Dehn). This is in contrast to an explosively formed projectile, which appears to have a definite mass from which one can measure velocity. Different penetration theories have been developed because of the differences between a kinetic energy (KE) projectile and those that resemble jets (Dehn). Figure 2.4 shows a cut away view of a typical CSC (Cooper).
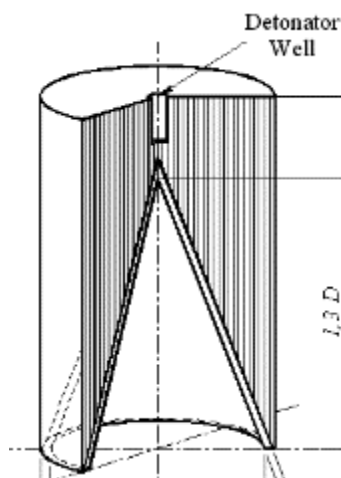
Figure 2.4. Cross sectional view of a typical CSC (Cooper)

Note that as the detonation wave expands spherically from the detonator well, the point of initiation, the liner is driven in a direction parallel to the direction of the expanding shockwave.

Hydrodynamic theories have been preferred for jets while other theories have been used to predict performance of bullets and fragments. Classical mechanics first attempted to describe the behavior of projectiles and their targets by analyzing the behavior of particles. This gave way to continuum mechanics, which attempts to resolve the kinematics of the entire object being studied by treating it as a continuous mass, as opposed to discrete particles (Raymond). Euler systemized the Lagragian and Eulerian viewpoints for these two methods (Dehn). Both of these viewpoints have been used in hydrodynamic and KE projectile penetration theories. Dehn's report, *A Unified Theory of Penetration,* continues to discuss previous efforts to describe the penetration of various projectiles while attempting to formulate a single theory that applies to all types of penetrators from a unified viewpoint.

Dehn noted that friction between the projectile and target was influential in the final stage of penetration while citing previous work on long rod penetration for a rod that was longer than the thickness of the target. The defeat of the rod was attributed to the friction between the target and the rod due to the rod being able to exit from the rear of the plate but not passing through completely, leaving the rod protruding from both the front and rear of the target. However, friction is considered negligible during most of the projectile's motion, particularly for metal targets and projectiles, according to several more sources Dehn used in his report (Dehn).

Energy from the projectile transferred to the target through heating and additional deformation was also unaccounted for by Dehn. According to Dehn, these two processes do not contribute to the penetration, which is "…complete in tens of hundreds of microseconds" (Dehn). The eventual redistribution of energy throughout the target was also ignored for the same reason. Dehn also worked under the assumption that the target and projectile are incompressible solids.

Additional assumptions include that all of the target forces were on the front of the target, the pressure on the sides and the rear of the projectile were zero, and the pressure gradient along the projectile, in force per unit volume, would be equal to equation 2.

$$P_g = p/L \qquad (2)$$

Equation 2 assumes that the volume of the projectile is equal to the cross sectional area times the length of the projectile. Multiplying equation 2 by the volume is equal to the pressure over the cross sectional area. Work cited by Dehn has shown that this is equal to approximately 3 times the ultimate yield strength, or elastic limit, of the target. Another sources claimed that this pressure can be as high as 100 times the yield strength of the

target (Novokshanov and Ockendon), though this number was stated for CSC and penetration was treated as a localized high pressure at the penetrator and target interface. Later in Dehn's report a series of tests are described where a long rod penetrator struck steel, aluminum, and copper targets at different speeds. Dehn comments on how target density is not the only factor involved in resisting penetration. This was made obvious by examining the penetration into copper and comparing it to the performance in aluminum and steel, two material which are less dense than copper, but stronger in terms of penetration resistance. The density of the copper was not able to compensate for its lack of strength and suffered a greater penetration than the other two materials.

The report by Dehn also included a brief survey on penetration theories. These theories largely did not define different types of steel and described the density of the target as the defining trait. Sources in Dehn's report did note that even though some materials like lead have a higher density than steel, penetration into lead is significantly greater. To explain this difference, experiments cited in Dehn's paper divided the penetration of the projectile into two different stages: primary and secondary penetration.

To summarize the conclusion from a previous attempt to explain this is that the projectile velocity of will be greater than the velocity of the penetration. At that time, the long rod penetrator will be eroded and this region can be classified as primary penetration. As the penetrator reaches the end of primary penetration, and "…plastic flow forward probably continues…" until the pressure is reduced to the elastic limit of the target. This was called secondary penetration and was thought to occur because the target was assumed to have forward momentum. Because the elastic limit in steel is higher than that of lead,

secondary penetration is less in steel that it is in the lead, explaining the deeper penetration (Dehn). Dehn presents another equation, shown in equation 3.

$$P = L\sqrt{\rho_j/\rho_t} \tag{3}$$

Where P is the penetration, L is the length of the penetrator, and ρ_j/ρ_t is the ratio of the penetrator to the target density. As the reader can see, this equation ignores the velocity, strength, viscosity, and any other property that might have effect on the depth of penetration. It is important to note that these equations were derived from experimental data gathered from CSC and long rod penetrators. Equation 3 works under the assumption that the yield strength of the target is zero when compared to the yield strength of the penetrator (Kalia). This equation has shown up in several other theories as well as modifications to add additional variables and constants, including accounting for non-negligible yield strength (Novokshanov and Ockendon) (Poole). Equation 4 is an example of one these early equations, developed by Pack & Evans in 1951, with added variables to account for the material target strength (Walters).

$$P = \left(\frac{\rho_j}{\rho_t}\right)^{\frac{1}{2}} L \left(1 - \frac{\alpha Y}{V^2 \rho_j}\right) \tag{4}$$

Where Y is the yield strength of the target and α is the velocity gradient of the jet. One year later, terms for the resistance of the jet and target to plastic deformation were added by Eichelberger & Pugh (Novokshanov and Ockendon). Equation 5 shows the updated equation.

$$\frac{1}{2}\rho_j(V-U)^2 + \sigma_j = \frac{1}{2}\rho_t U^2 + \sigma_t \tag{5}$$

Some of these theories are considered when examining the results of the experiments in this thesis. It is important to note the only changing variable between the tests is the size of the LSC and the target material.

2.4. HISTORY OF THE SHAPED CHARGE

Simply put, a shaped charge uses the geometry of the explosive charge for a desired effect. Max Von Foerster is credited with discovering the effect of a hollow charge in 1883 while experimenting with compressed nitrocellulose. However, Charles E. Munroe is perhaps the name most commonly associated with the shaped charge. In 1900, his shaped charge design was described as being able to defeat four inches of iron and steel and was probably the first successful use and demonstration of a metal lined shaped charge; because of this, the effect of a charge with a metal lined cavity has since been known as the "Munroe Effect". Munroe describe this effect as the reinforcement of shock waves in a hollow charge that would concentrate the explosive effects (Smith). Shaped charges were used extensively in World War I and World War II in torpedoes, rifle grenades, and rockets. After the war, shaped charges were applied to civilian applications. Some of the uses include oil well completions, steel furnace tapping, and in scientific research (Kennedy). More recently, research has been conducted in penetration theories of shaped charges, numerical modeling of the charge (Poole), and optimization of targets against a shaped charge (Hussain, Hameed and Horsfall). Currently, many different types of shaped charges are available from various manufacturers. The most common type is the CSC. The type of shaped charge that this thesis focusses is the LSC. Both types of shaped charges can be produced with sheaths or liners made from lead, aluminum, copper, silver, or steel.

2.5. LINEAR SHAPED CHARGE

LSCs have been used in demolition, aerospace, and research applications. Figure
2.5 shows an LSC not unlike the charges that were used in this thesis. The figure is typical
of an LSC and serves to demonstrate the basic components of an LSC (Smith).
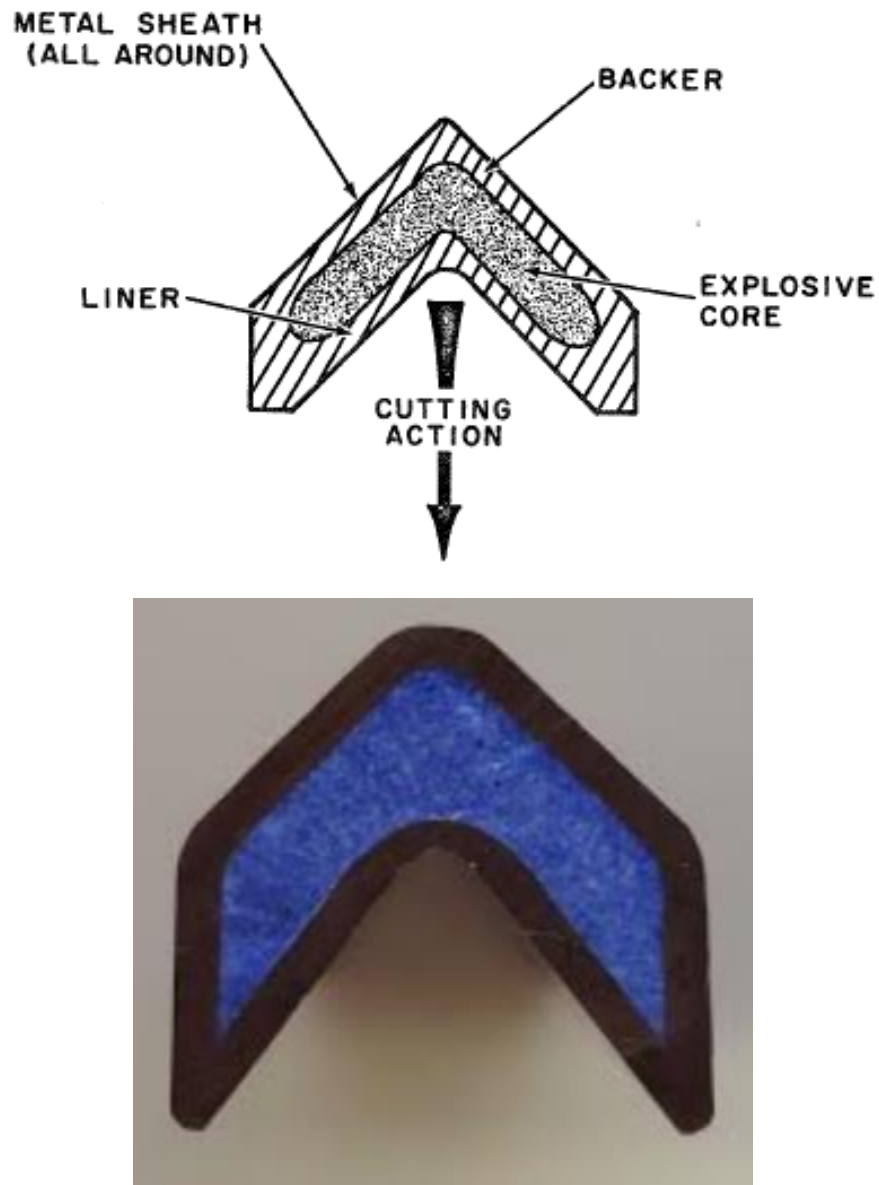
Figure 2.5. Typical LSC showing common components and direction of Penetration
Performance (Smith) above a picture of an LSC

Compared to a CSC's top-down initiation, an LSC's shockwave travels in a direction normal to the direction of jet travel. This means an LSC jet is not identical to, and cannot be compared to a jet from a CSC (Burch). An early stage of penetrator formation can be seen in, Figure 2.6, a high-speed photograph captured during previous work at Missouri University of Science and Technology (Lim). LSCs have also been found to produce a projectile much slower than their CSC counterpart does.

Figure 2.6. An LSC soon after detonation. The projectile will travel in a direction perpendicular to the detonation wave (Lim)

The first LSCs worked on the same principles as modern designs but lacked the optimization that current devices went through. As researchers figured out optimum angles, core loads, and material, users saw performance increase. Figure 2.7 shows the evolution of the LSC into a more familiar modern shape shown in Figure 2.8 (Johnston and Lim).

"Kidney" Shaped

Configuration I

Configuration II

Configuration III

Configuration IV

Configuration V
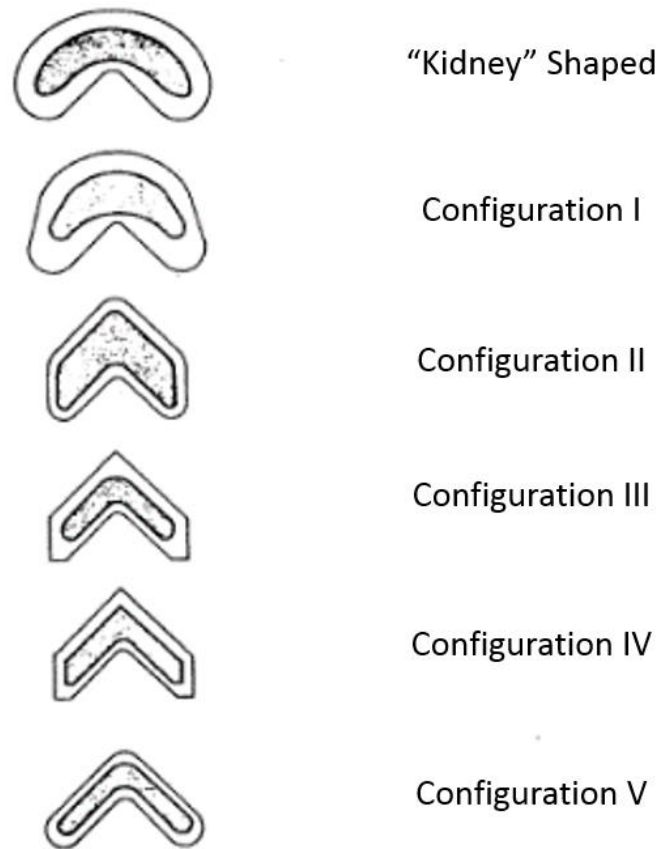
Figure 2.7. Cross-sectional view showing the evolution from an Early LSC Design
(Johnston and Lim)
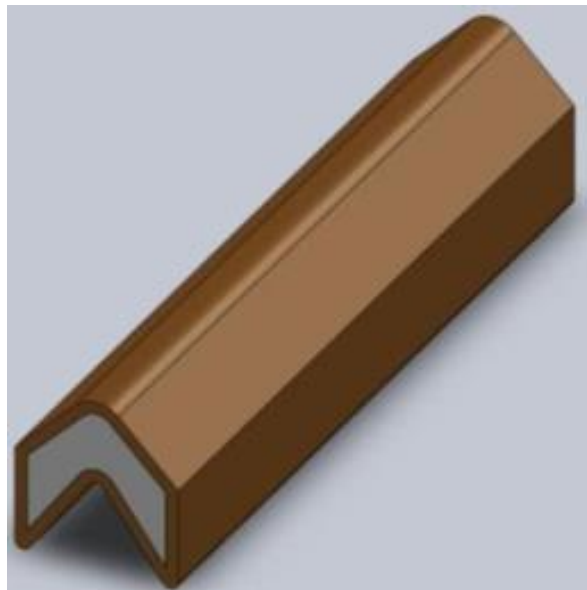
Figure 2.8. CAD representation of the LSCs used in this experiment (Johnston and Lim)

Modern commercial LSCs are often lined with aluminum, steel, copper, or lead. The liner choice is often based on the needs of the user. For example, a lead lined LSC can be flexible and will function relatively well with little to no standoff; environmental regulations may limit the use of lead however. An LSC also has a variety of options when choosing an explosive fill. Common core loads include pure and sensitized versions of RDX and HMX, HNS, and TNT based melt-cast formulations. The manufacturer of the shaped charges used in this test produces charges with a core load from 25 grains per linear foot up to 60,000 grains of explosives per linear foot. Missouri S&T research in the past cover topics from liner collapse to detonation methods have used this particular brand of LSC.

3. INTRODUCTION TO TARGETS

3.1. TARGET CLASSIFICATIONS

Steel can be classified based on chemical composition, production process, or variety of other methods. Different countries also have their own way of classifying metal material. Several organizations have attempted to standardize the classification system because of the variety of options. Two of the most common classification systems describe steel and aluminum based on their chemical composition, which relies on carbon content and additional alloying metal content (Brammfitt and Benscoter). It is important to note that there are many other classes of steels other than the ones described here. Figure 3.1 is an example of the complexity involved when classifying steel.

3.1.1. Carbon Steel. Carbon is generally the most important alloy when it comes to commercial steel. Hardness, strength, and hardenability increases as carbon content increases. However, as carbon content increases, brittleness and weldability decreases. Controlling the carbon content is one way steels are engineered to get the desired performance. The carbon content is a factor when classifying commercial steel into one of the following three groups:

1. Plain carbon steel

2. Low-alloy steel

3. High-alloy steel

The next few sections will further detail these three classes of steels and provide typical applications of the steels. The sections discussing the materials used in this test will later reference these classes and define the more specific classifications. Cast iron is another class of steel.

3.1.1.1. Plain carbon steels. Plain carbon steels typically contain less than one percent carbon. Manganese, sulfur, phosphorus, and silicon are also added in small amounts to the steel. The carbon content is the biggest influence on the characteristics of these steels while the other alloying components have a smaller impact on the material (Brammfitt and Benscoter).

Within the plain carbon class of steels, exists four sub-categories. These groups are low, medium, high, and very high. Again, this is based on the carbon content of the steel. Low plain carbon steel is more commonly known as mild steel. According to the American society of metals, low carbon steel has a carbon content of less than 0.20 percent. Medium and high-carbon steel have a carbon content from 0.20 to 0.5 and above 0.5 percent, respectively. As the carbon content increases with these grades, so do the hardness and tensile strength. However, ductility and weldability decrease as a result (Brammfitt and Benscoter).
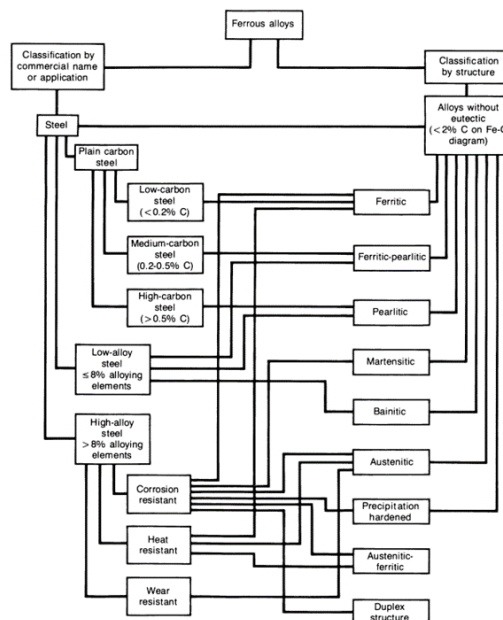
Figure 3.1. Example of steel classification chart from ASM (Brammfitt and Benscoter)

3.1.1.2. Low-alloy steel. This next class of steels is designed for welding applications. Typical steels in this class have chromium, nickel, manganese, silicon, and molybdenum. Low alloy steels are those with less than 8% alloying elements. These steels have increased corrosion resistance compared to the plain carbon steels (Brammfitt and Benscoter).

3.1.1.3. High-alloy steel. Stainless steel is the main constituent of this class of steel. Stainless steels have at least 12 percent chromium and are typically made with a high percentage of nickel. Stainless steel is further divided into three types: martensitic, ferritic, and austenitic (Brammfitt and Benscoter).

3.1.2. AISI/SAE Classification System. Plain carbon steel is often defined by the American Iron and Steel Institute (AISI) and the Society of Automotive Engineers (SAE). The classifications for almost identical so users will often see the specifications designated as AISI/SAE steels followed by their steel code number. AISI adds a letter to the specification that indicates the process used to make the steel, which is the main difference between the two (Smart and Steber).

3.1.2.1. Steel. AISI uses a numbering system to define and classify types of steel. The system is based on a four-digit number system with the first two digits categorizing the steel into a basic group. The next two numbers indicating carbon content. For example, 1018 steel is classified as a plain carbon steel and typically contains 0.18% carbon. There are five subclasses of plain carbon steel within the AISI/SAE classification system, 10xx, 11xx, 12xx, 13xx, and 15xx, which vary mainly by manganese content (U.S. Department of Transportation: Federal Aviation Administration).

Stainless steel is classified in a three digit numbering system, as opposed to four digits. A stainless steel used in this experiment belongs in the 300 series class. The 300 series stainless steel is reserved for austenitic chromium-nickel alloys (U.S. Department of Transportation: Federal Aviation Administration).

3.1.2.2. Aluminum. Aluminum is also classified with a four-digit system. The first two digits describe the basic class while the last two describe an alloy content, similar to the four digit steel classifications. Subclasses of aluminum include pure, copper alloys, silicon alloys, and zinc alloys, to name a few (U.S. Department of Transportation: Federal Aviation Administration).

3.1.3. American Society for Testing and Materials Classification System. The American Society for Testing and Materials (ASTM) also provides steel classifications in addition to more than 12,000 other metal products. Unlike AISI/SAE, ASTM bases classification of steel and aluminum on the product and application (Brammfitt and Benscoter). A36, a popular structural steel, is the ASTM classification for carbon structural steel. Other steel codes from ASTM will also start with an A (U.S. Department of Transportation: Federal Aviation Administration).

4. TARGET MATERIALS

This section discusses the five targets chosen for the tests and some typical uses, as well as how they are used in industry. The target materials were procured with mill specifications that detail the material properties when possible. However, this led to some targets of the same material to have slightly different properties. For example, the A36 steel targets in this experiment had a yield strength between 38,600 to 41,300 psi. The material that is currently used by the LSC manufacturer for testing is 1018 steel and is discussed first.

4.1. 1018 STEEL

1018 steel was the type of steel used initially by the LSC manufacturer when testing their devices. The advertised penetration data was taken from tests into this type of steel. It is a type of carbon steel that is commonly used for fabrication. The American Society for Metals defines carbon steel as steel that has a maximum of about 2.0% carbon. (Dossett and Boyer). 1018 is classified as low carbon steel, which means it contains between 0.14 and 0.20 percent carbon, by weight (MatWeb). This steel is typically used for machine parts such as gears, ratchets, pinions, and components of tool and die sets (ASTM International). It is also used in applications that do not require a high weight-to-strength ratio, but still require high strength and durability (O'Neal Steel). It is the most commonly available cold-rolled steel and, chemically, very similar to A36 Steel, which will be discussed in the next section. Specification 1018 is in the 10xx series of AISI steel and designated as non-sulfurized carbon steel or plain carbon steel (U.S. Department of Transportation: Federal Aviation Administration).

4.2. A36 STEEL

Researchers at MS&T previously tested this type of low carbon steel with the LSC manufacturer's devices. A36 is the most commonly available hot-rolled steel. It is used for beams, angles, channels, and can be supplied in multiple other shapes. It can also be used in structural applications such as in buildings, cabinets and enclosures, and pipes (ASTM International). Through an internet search and the ASTM data sheet that was supplied with the targets, material properties were established that would be used in the analysis of the LSC penetration.

4.3. 4340 STEEL

4340 steel is known as a low alloy steel. Following AISI naming convention, the first two digits in 4340 designates it as Nickel-Chromium-Molybdenum alloy steel, while the last two reveals the carbon content, which is approximately 0.40 percent (U.S. Department of Transportation: Federal Aviation Administration). 4340-alloy steel is used in aircraft landing gear, transmission gears, and other structural parts. This steel has been used as targets for shaped charge testing in the past. The steel manufacturer supplied ASTM 829, which is the specification for alloy structural steel plates (ASTM International). The properties from this data sheet are used in the analysis.

4.4. 304L STAINLESS STEEL

Grade 304 stainless steel is known to be the most commonly used and available stainless steel. It is known as the standard 18/8 stainless because of its chemical composition. The 304 grade is further divided into a 304L and a 304H grade, indicating a

low and high carbon version, respectively. Typical applications of 304 stainless steel include food processing equipment, chemical containers, and architectural (Goodfellow). A249 is the specification for welded austenitic steel (ASTM International) and the certification that was delivered with the targets. The analyses were performed on properties from this data sheet.

4.5. 6061-T6 ALUMINUM

The last type of material chosen for the initial tests was 6061-T6 aluminum. This type of aluminum is an aluminum-magnesium-silicon alloy that was first introduced in 1935 that fit industries need for a medium strength metal that could be welded. This alloy has good corrosion resistance, even after welding, and is easily hot-worked. These properties made it ideal for early marine and railroad applications (Sanders). This aluminum belongs to the 6000 series of aluminum, which are the magnesium and silicon alloys. The 6000 series aluminum typically has good forming qualities and medium strength. The –T6 suffix refers to the solution heat treatment applied to the product as well as artificial ageing (U.S. Department of Transportation: Federal Aviation Administration). This target material was provided with an ASTM B221 12 data sheet by the material manufacture. ASTM B221 12 is the standard specification for aluminum and aluminum-alloy extruded bars, rods, wire, profiles, and tubes (ASTM International).

5. TEST SET-UP

5.1. LINEAR SHAPED CHARGE SELECTION

The LSCs used in this experiment were chosen because they are common in industry and follow the manufactures request for these particular sizes, liner material, and core load. All of the devices used in this experiment had an RDX core load with a copper liner. The charges were also all from the same lot, passed the company's quality control inspections, and can be considered identical to charges that are used in industry.

The first LSC chosen was the 600 grain per foot charge. The 600 gr/ft. charge is advertised to cut 0.70 inches of 1018 steel at the manufactures recommended standoff. The second and third charges were 2,000 gr/ft. and the 4,000 gr/ft. LSC, respectively. The 2,000 gr/ft. LSC is advertised to cut 1.50 inches of 1018 steel at the manufactures recommended standoff and the 4,000 gr/ft. LSC is advertised to cut 2.00 inches at the recommended standoff.

5.2. JOINING THE LSC TO THE TARGET PLATE

All of the LSCs were cut to a length of twelve inches. The targets were twelve inches long and four inches wide. The steel targets for the 600 gr/ft. charge were one inch thick while the aluminum target was two inches thick due to the assumed increase in penetration. Steel targets for the 2,000 gr/ft. shaped charge were two inches thick and the aluminum target was three inches thick. The steel targets for the 4,000 gr/ft. LSC were 2.5 inches thick and 4 inches for the aluminum target. The target thickness for each test is displayed in Table 5.1. The length of the target was matched to the length of the LSC to keep set up consistent. The lengths of the LSC and target were also made equal so the

amount of overlap, of either the charge or the target, would not need to be changed for each

charge.

Table 5.1. Table showing the thickness of the different targets used in each test

Target Thickness (in.)					
LSC (gr/ft.)	A36	1018	4340	304	6061
600	1.0	1.0	1.0	1.0	2.0
2,000	2.0	2.0	2.0	2.0	2.5
4,000	2.5	2.5	2.5	2.5	4.0

Ideally, larger targets would be used to minimize the effect that inertia of the target

has on penetration. However, since only the cut portion of the target was analyzed, not the

brittle fracturing that may follow, the effect of confinement was not analyzed.

Figure 5.1 shows the typical set-up of the LSC on the target. The standoffs clip on

to the LSC then the assembly is taped to the target. The standoffs used in this test are used

by the LSC manufacturer and are commonly used in the demolition industry. The standoffs

were designed to not interfere with the penetrator formation or path. Other low-density

standoffs, such as PVC pipe and foam, can also be used.
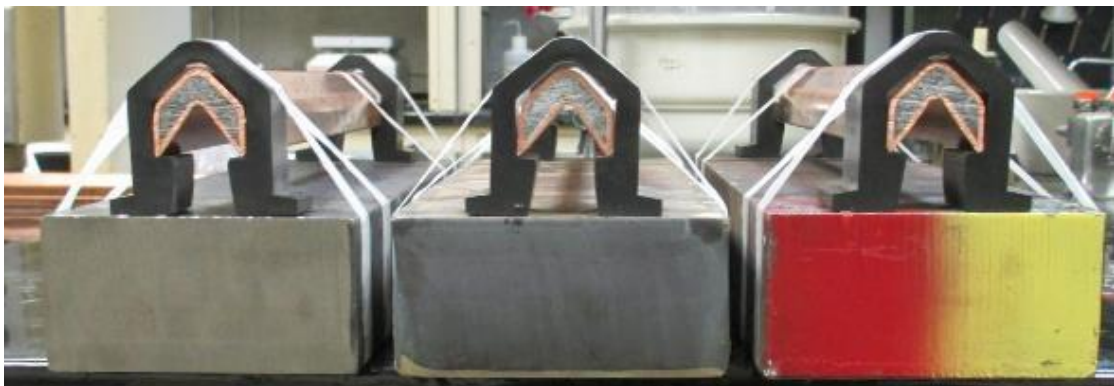
Figure 5.1. End view showing the typical setup of the LSC onto the target plates

5.3. TEST SITE

The test site is an outdoor test range owned and operated by the manufacture of the LSC. The test site is covered in sand and frequently leveled and smoothed by the owner to fix any craters left by previous tests. One of the assemblies, in Figure 5.1, was placed on the sand and then the initiator was attached as described in the next section. This type of set-up was used for all of the tests.

5.4. INITIATION OF THE LSC

An LSC can be initiated in a number of ways. The most common method of initiation is a point initiation on an end of the charge against the exposed explosive. Figure 5.2 shows three additional methods that achieve detonation; but these are not as effective. (Ortel). Users of these charges sometimes use a booster in addition to the detonator to assure a proper detonation is achieved. A detonator and a booster may also be used to initiate the device from the top of the charge.
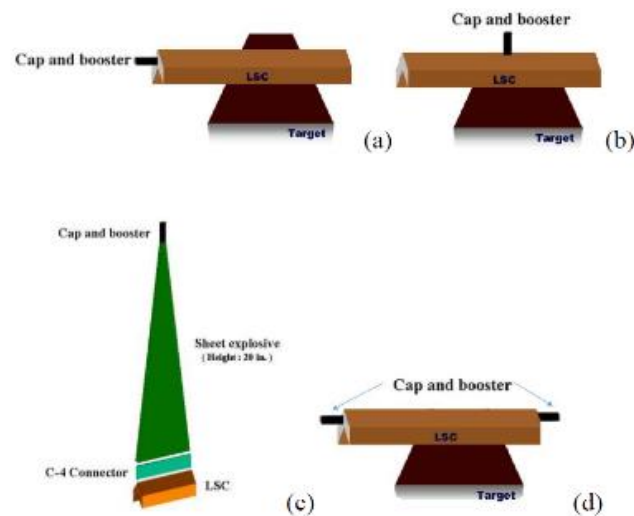
Figure 5.2. Four different methods for initiating an LSC. A) Point, B) top C)Planar top, D) dual end-to-end

Point initiation was the method chosen for this experiment because this was standard practice at the test facility. The point initiation of the charge was achieved through a number 8 detonator taped to one end of the charge. The tape used to hold the detonator is seen on the right side of Figure 5.3. To the author's knowledge, this method of initiation had not previously been an issue and did not create any for this series of tests. The preferred method of detonation would be to use an eight to ten gram booster to initiate the LSC. Using a booster increases the surface area of the LSC that is initiated creates a planar shockwave within the LSC sooner, reducing the amount of run-up. However, a booster was not available to the author at the time of these experiments.

Initiation End

Figure 5.3. View from above showing a typical setup of an LSC on a target block and the position of the detonator

6. RESULTS AND DATA ANALYSIS

6.1. RESULTS

Depth of penetration measurements were recorded by the author for each of the shot targets. The method for describing the average penetration into the targets is described in following sections. The results, shown in Table 6.1, were then compared to the target's material properties to examine any relationships between the properties and penetration resistance.

Table 6.1. Depth of average penetration into each target material

Average Penetration (in.)

LSC (gr/ft)	6061	A36	1018	304	4340
600	1.24	0.85	0.77	0.67	0.62
2,000	2.52	1.61	1.61	1.33	1.29
4,000	3.54	2.02	2.05	1.90	1.66

The aluminum target sustained the most penetration by all three LSC sizes. The penetration was roughly twice that of the most resistant material, 4340 steel. The 304 stainless material was the second most resistant material and had almost the same amount of resistance to penetration as the 4340. The A36 and 1018 material had identical penetration for the 2,000 gr/ft. and saw nearly identical penetration in the 4,000 gr/ft. test, where A36 was slightly more resilient. However, during the 600 gr/ft. test, the 1018 target saw less penetration that the A36 target.

6.2. DEFINING THE CUT REGION FOR ANALYSIS

The portion of the cut that was examined in these tests was only the part of the target that was cut by the LSC blade. Most of the targets were completely cracked in half. Additional brittle fracturing of the target was not included in measurement. Most likely, this shock-induced fracturing occurs because of the penetration of the LSC jet, gas pressure, and momentum of the two sides of the block, which is a function of the relatively small target size. Another contributing factor in target fracturing is the longitudinal sound speed of the target material (Pazienza). The blade enters the target at a velocity of roughly three to four thousand feet per second. The target absorbs some of the energy of the blade and beings to deform plastically. As it slows down, the blade continues to act as a wedge and drives the two sides apart. By this time, the expanding gas from detonation and the blade slows to below the crack tip velocity and the target fractures. A target that was completely fractured can be seen in Figure 6.1. .a significant amount of run-up can be seen on the right side of the target, which is the end the LSC was initiated. A target that was not fractured into two pieces can be seen in Figure 6.2. This photograph was taken on the end which initiation took place. The copper penetrator can be seen within the penetration cavity of one of the aluminum targets that failed to fracture completely.

Figure 6.1. Target typical of an LSC test. Note that this target fractured completely and did not need to be cut post-test
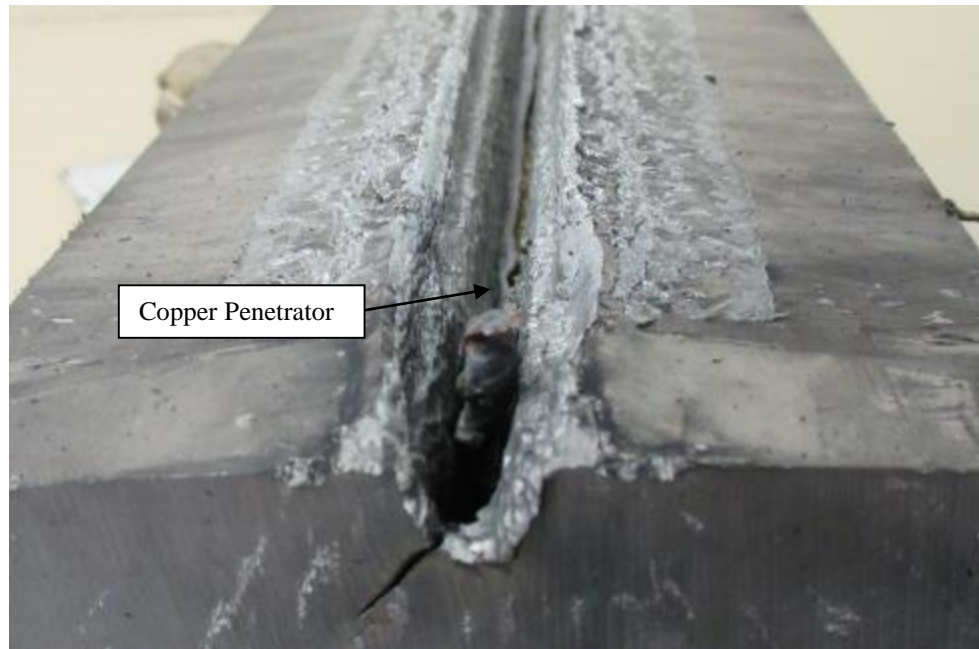
Figure 6.2. View from the end of a target that was not completely cut or fractured as a result of an LSC test

6.3. DETERMINING PENETRATION

After the target was shot, the two halves were recovered. If the LSC did not sever the target, the target was cut in half to expose the cut faces. This was done to get the most accurate measurement of the penetration. The method of analysis is one that researchers at Missouri S&T had used previously (Phelps, Nolan and Baird). Details of this method are in Appendix A. After the test, the two halves of the target were cleaned and a picture of the target half was imported into a computer aided design (CAD) program to gather penetration data. Penetration depth was imported into a spreadsheet program, shown in Table 6.2, and performance characteristics were determined. The program is able to output the different aspects of the cut, such as an average penetration. The table is an example of what a typical table looks like after the data points are input. Note that not all of the data points were shown in this table. The user has the option of choosing any of the sizes made by the

manufacturer and the spreadsheet will indicate how the charge performed compared to the advertised performance. The spreadsheet also classifies each data point into one of the three stages of LSC penetration: run-up, penetration, and run-down.

Table 6.2. Table showing penetration data inputs

LSC (gr/ft)		600
Acceptable Deviation (% of Max Penetration)	25	0.181175
Max Penetration (in)		0.7247
Target Penetration (in)		0.7

Data Point	Penetration Value (in.)	Cut Type
1	0.2048	Run-Up
2	0.3969	Run-Up
3	0.4965	Run-Up
4	0.6162	Penetration Range
5	0.6533	Penetration Range
6	0.6354	Penetration Range
7	0.6663	Penetration Range
8	0.672	Penetration Range
9	0.6574	Penetration Range
10	0.6341	Penetration Range
11	0.6947	Penetration Range
12	0.6937	Penetration Range
13	0.6862	Penetration Range
14	0.7014	Penetration Range
15	0.7006	Penetration Range
16	0.6939	Penetration Range
17	0.6869	Penetration Range

These measurements comprised of forty equally spaced data points taken along the length of the cut from where depth measurements can be taken to approximate the penetration of the copper blade. Having a digital record in a spreadsheet allows the user to revisit the data and pull different metrics or inspect different aspects of the cut that were dismissed during the initial inspection. Typically, before this method, a user who was

interested in the penetration depth would visually inspect the target after the test and a few penetration points were taken along the cut, then the target thrown out. This can lead to biased data from the person who is measuring or missed opportunities to gather additional data on different aspects of the target before it is disposed of. Keeping a digital record of dimensions and other unusual observations can save the researcher from doing unnecessary tests in the future.

6.4. AVERAGE PENETRATION VERSUS MAXIMUM PENETRATION

One of the measures of performance examined in this thesis was a metric called average penetration. This is the average depth of the portion of the penetration that was within 25% of the maximum depth achieved. This can be better visualized below. Figure 6.3 was one of the targets that had to be cut in half after a test. The targets often experienced a large amount of deformation that made it difficult to make a clean cut through the center. The author regularly had to discard one-half of the target because of the damage to the other half from the difficulty in cutting such distorted pieces. Figure 6.3 is half of the stainless steel target tested against the 4,000 gr/ft. LSC.
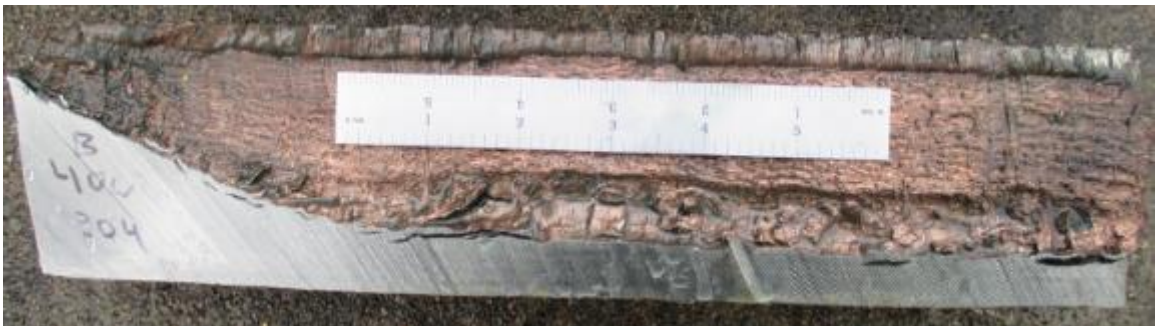
Figure 6.3. Target that was cut in half in order to examine the penetration

Figure 6.4 shows a trace of the same target along with a trace of the penetration. These data points are from the previous target and show the extent of the cut. Note that the image was mirrored for analysis.
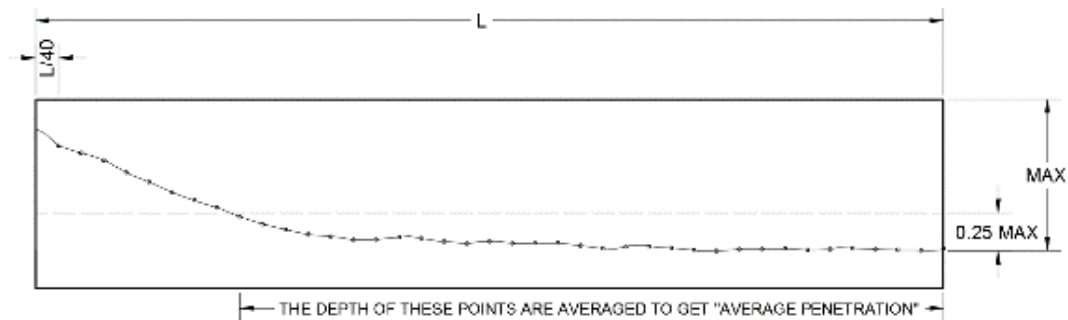
Figure 6.4. Data points collected from the depth of penetration of the target in the previous figure

Table 6.2 compares the difference between the points with the maximum penetration in any of the tests against the average penetration obtained using the previously mentioned method. The mean penetration was, on average, 8% lower than the maximum obtained when looking at the point that penetrated the furthest.

The average penetration was chosen because of the chance that the maximum penetration was not representative of the cut. In addition, in real world applications, a user would be more interested in what the majority of the charge was capable of, not just the maximum penetration of one small portion. Figure 6.5 demonstrates the difference between the depth of maximum penetration and the average penetration. On this particular target, 88% of the data points were within 25% of the maximum depth cut, which gives a better picture of what the LSC is capable of cutting. The figure shows a portion of the actual output once the data points are entered into the spreadsheet. The reader can see how recording performance based on maximum penetration could affect LSC selection.
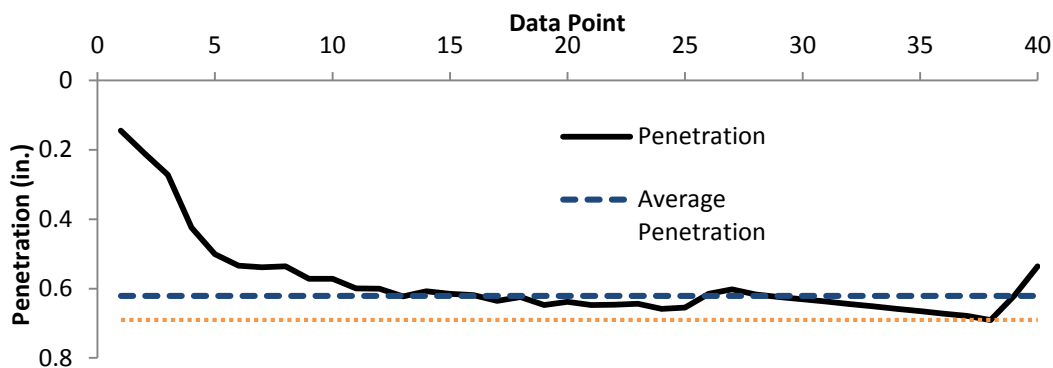
Figure 6.5. Spreadsheet output displaying the average penetration in relation to the maximum penetration

6.4.1. Penetration into 304 Stainless Steel. Each stainless steel target required cutting in half after the test in order to fully examine the cut in the method described earlier. The target for the 4,000 grain LSC had to be cut in half after the piece was recovered post-test. This piece is shown in Figure 6.3. All three targets were measured and downloaded in the spreadsheet to analyze the cut. The largest difference between the maximum and the average penetration into the stainless steel was 9%. This difference occurred in the target that was penetrated by the 2,000 gr/foot LSC. This is equal to roughly a tenth of an inch difference between the maximum and average penetration. Table 6.3 shows the Penetration values in the 304 steel of this test as well as the other two tests into this material. Pictures of the targets are displayed in Appendix B.

Table 6.3. Differences between the average and maximum penetration into 304L Stainless Steel

304 Stainless Steel: Maximum vs. Average Penetration			
LSC (gr/ft)	Maximum	Average	Difference (in)
600	0.72	0.67	0.05
2,000	1.46	1.33	0.13
4,000	2.02	1.90	0.12

6.4.2. Penetration into 6061-T6 Aluminum. All of the aluminum targets severed in half during the test. The three targets had average penetrations that were all within 7.5% of the maximum penetration. Figure 6.6 shows an example of a target that was penetrated by the blade from a 2,000 gr/foot LSC, which showed an approximately 0.2" inch difference between the average and maximum penetration. Photos of the other targets are displayed in Appendix C.

Figure 6.6. Aluminum target that was recovered after 2,000 gr/ft. LSC penetration

Table 6.4 shows the maximum and average penetration of the LSC into the aluminum target. Note that the aluminum, which is an outlier when comparing properties compared to the other target materials, shows a difference between these two metrics that is relatively close to the stainless steel.

Table 6.4. Maximum vs. average penetration into the 6061 aluminum targets

6061 Aluminum: Maximum vs. Average Penetration			
LSC (gr/ft)	Maximum	Average	Difference (in)
600	1.33	1.24	0.09
2,000	2.70	2.52	0.18
4,000	3.75	3.54	0.21

6.4.3. Penetration into 4340 Steel. Two of the three 4340 steel targets were severed in two pieces after the test. The target plate for the 600 gr/foot LSC was cut in half after the test to examine the penetration. Half of this target was damaged and discarded. See Appendix D for photographs of the 4340 steel targets. Table 6.5 shows the difference between the average penetrations versus the deepest point of penetration. The target for the 600 gr/ft. LSC had the biggest percentage difference between the maximum and average penetration of the five target materials initially tested. Even with the relatively large difference between maximum and average penetration, this target still had 87.5% of its data points within the average range. The data points for all 4340 steel are in Appendix A.

Table 6.5. Maximum vs. average penetration into the 4340 steel targets

4340 Steel: Maximum vs. Average Penetration

LSC (gr/ft)	Maximum	Average	Difference (in)
600	0.69	0.62	0.07
2,000	1.40	1.29	0.11
4,000	1.80	1.66	0.14

6.4.4. Penetration into A36 Steel. Only one of the A36 targets needed to be cut after the test. Again, this was the target for the 600 gr/foot LSC. Half of this target could not be used for analysis as it was too damaged. Pictures of the A36 targets are displayed in Appendix E. The differences between the average and maximum penetration are shown in Table 6.6. These differences are about 9 percent for the three targets. A smaller difference means that the LSC is penetrating more consistently throughout the length. The average penetrations spanned almost 90% of the length of the target. This means that almost 90% of the penetration into the target is within 25% of the maximum penetration.

Table 6.6. Maximum vs. average penetration into the A36 steel targets

A36 Steel: Maximum vs. Average Penetration

LSC (gr/ft)	Maximum	Average	Difference (in)
600	0.93	0.85	0.08
2,000	1.76	1.61	0.15
4,000	2.20	2.02	0.18

6.4.5. Penetration into 1018 Steel. The penetration into the 1018 was also found to be relatively consistent. This material had the smallest differences between the average and maximum penetration. Even though the difference in average and maximum penetration seems rather small, using this performance metric is believed to yield data that is representative of the overall performance of the charge. Table 6.7 below shows the numbers for the 1018 Steel. Images of the 1018 can be seen in Appendix F.

Table 6.7. Maximum vs. average penetration into the 1018 steel targets

1018 Steel: Maximum vs. Average Penetration

LSC (gr/ft)	Maximum	Average	Difference (in)
600	0.83	0.77	0.06
2,000	1.72	1.61	0.11
4,000	2.18	2.05	0.13

6.5. DENSITY

The first property compared to penetration was the density of the target. The penetration depth that was used was the average penetration that was described in section 6. Individual target properties, such as density, hardness, and moduli, could not be controlled and adjusted, so the information was graphed and any correlations were analyzed. The first analysis will identify if a change in density of the target correlated to a change in the penetration of the LSC. The four steels used in this experiment had densities

typical of steel, which ranged from 0.283 to 0.289 pounds per cubic inch. The aluminum target had a density that was roughly a third of the steel. Table 6.8 shows the densities of the target materials. The densities are from the target manufactures certifications of that target material.

Table 6.8. Densities of the target materials

Material	Density (lbs./in^3)
6061 Aluminum	0.0975
A36 Steel	0.283
4340 Steel	0.283
1018 Steel	0.284
304L Stainless	0.289

The analysis uses the penetration data from the previous section. As seen in Table 6.7 and Figure 6.7, the densities of the steel targets were nearly identical while the penetration was not. A36 and 4340 had a density of 0.283 lbs. /in^3 and the density of the 1018 steel was 0.284 lbs. /in^3. However, the 2,000 gr/ft. shaped charge had an average penetration of 1.61 inches in the A36 and 1018 target, but only 1.29 inches in 4340, a material with the same density. The penetration of the 304 stainless was much closer to the depth seen in the carbon steels, A36 and 1018, even though it had the highest density. On average, there was a 28% difference in penetration between the A36 and 4340 targets, two materials with identical densities. Target density does not appear to influence the depth of penetration when examining only the steel targets. However, density may be a contributing factor when comparing results in steel against penetration in aluminum or other materials.
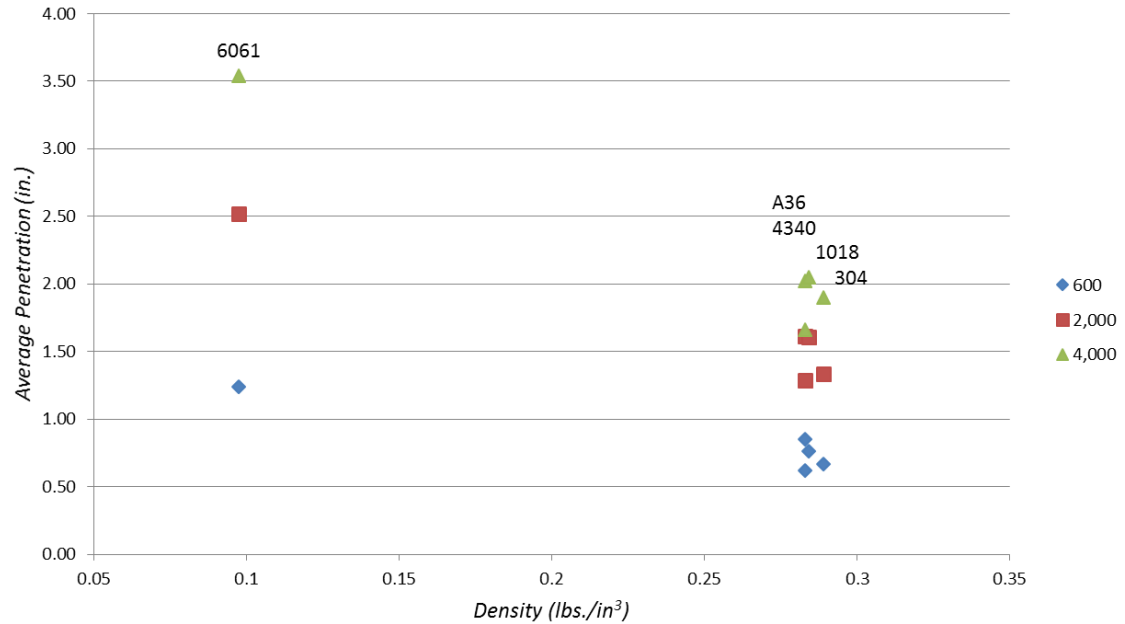
Figure 6.7. Average penetration vs. density into the fifteen targets. Note that the target material is defined above the group of points

6.6. YIELD STRENGTH

Yield strength is used to describe the stress at which point plastic deformation begins and the material will not return to its original shaped after the stress is removed. This happens after the material goes through the elastic region of deformation. With the targets used in this test, yield strength was reported using a 0.2% elongation, called the offset yield strength. On a stress-strain curve, the elastic region of stress is generally linear, so a line parallel to the elastic line is drawn intersecting at 0.2% on the strain axis. Where this line intersects the stress-strain curve is the said to be the yield strength. This relationship can be seen in Figure 6.8 (U.S. Department of Energy). The ultimate tensile strength is also shown in this figure, which is discussed in the next section.
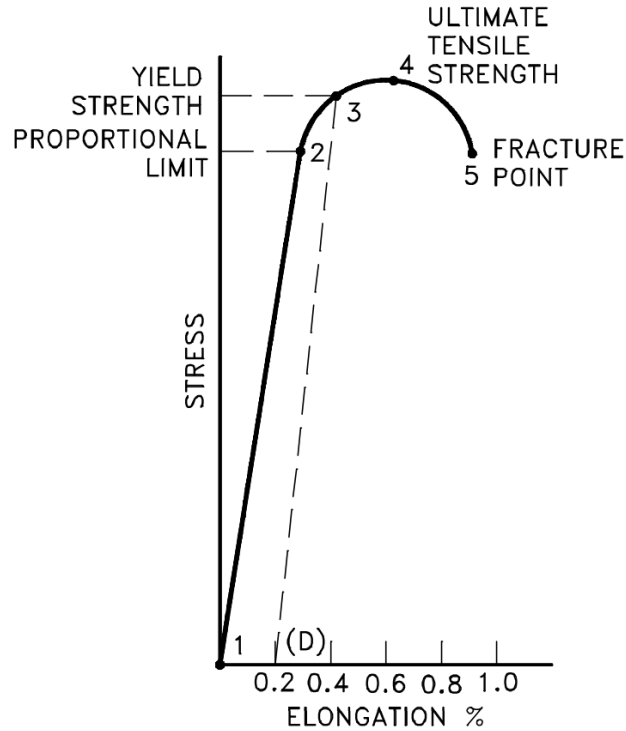
Figure 6.8. Stress-Strain curve showing the yield strength along with other material properties (U.S. Department of Energy)

Table 6.9 shows the yield strength of the materials used in this experiment. The data for 4340 was found after an internet search. All other target materials were supplied with a specification sheet from the manufacturer.

Table 6.9. Yield strength in pounds per square inch of the targets used in this test

Yield Strength in Pounds per Sqaure Inch

LSC (gr/ft)	A36	304	1018	6061	4340
600	38,600	44,410	45,000	48,350	72,800
2,000	41,188	41,800	45,000	45,600	72,800
4,000	41,300	44,420	45,000	47,600	72,800

Figure 6.9 shows the relationship between the yield strength, in psi, and the average penetration of the LSC. It is important to remember that some of the targets of the same

material were obtained with specifications from the mill reporting different material properties. The graph below shows the materials not vertically aligning because of these differences. Note that the x-axis starts at 35,000 psi. The yield strength is shown in kpsi to make reading the graph easier.
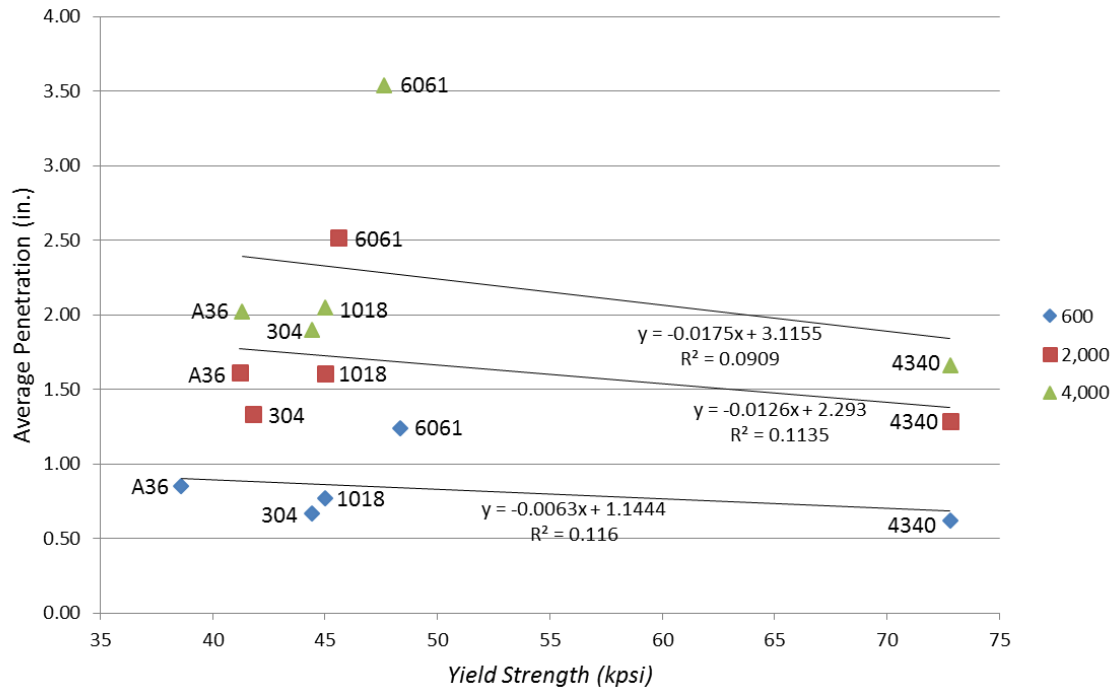
Figure 6.9. Average penetration versus the yield strength of the target

Looking at the graph and the table, it is apparent that an increase in yield strength does not necessarily indicate a decrease in penetration. This is the most obvious when focusing on the average penetration in the 4340. The yield strength of 4340 was almost twice as high as the other steels while the penetration was only a few percent less. The aluminum target also suggests that yield strength has a negligible effect on penetration. The aluminum has the second highest yield strength yet resists penetration half as well as the other targets. The aluminum target in this thesis is an outlier, both in material and in

performance against the LSC. However, the author found the same lack of correlation when analyzing only the steel targets. The yield strength versus penetration depth can be seen plotted again in Figure 6.10, this time without the aluminum.
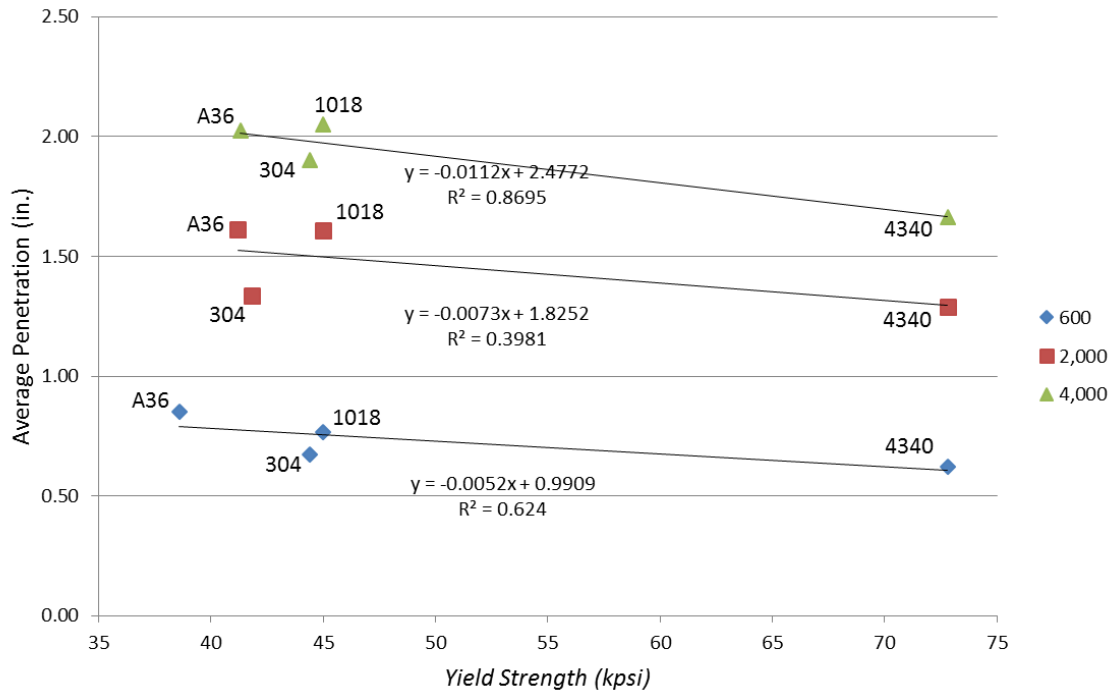
Figure 6.10. Average penetration versus the target yield strength with the aluminum target data removed

This graph continues to show why yield strength is not a good indicator of performance. The reader can see that there is a weak correlation and a shallow slope. The stainless steel has one of the lowest yield strengths but resists penetration just as well as the 4340. A36 and 1018 had almost identical penetration but different yield strengths, with the 1018 almost matching the yield strength of the stainless steel targets. The next material property examined was the ultimate tensile strength, which comes after the elastic region defined by the yield strength in a stress-strain curve.

6.7. ULTIMATE TENSILE STRENGTH

Ultimate tensile strength (UTS) describes the tensile stress that can be applied to a material before it breaks or fails. This is determined through a standard test and can vary across different material cross sections. It is a commonly used measurement in the description of metal and alloy properties. The UTS of the targets are displayed in kpsi in Table 6.10. These values for these targets, except for 4340, are from specification sheets supplied by the target manufacturer. The ultimate tensile strength is from an internet search for the target material.

Table 6.10. Ultimate Tensile Strength of the targets used in this experiment (MatWeb)

Ultimate Strength in Pounds per Sqaure Inch					
LSC (gr/ft)	*A36*	*304*	*1018*	*6061*	*4340*
600	59,400	91,200	65,300	51,800	161,000
2,000	67,500	89,200	65,300	49,100	161,000
4,000	66,800	91,200	65,300	51,700	161,000

In other words, the 4340 steel has a UTS almost 3 times higher than that of A36 steel. A better way to visualize these large differences is shown following, in Table 6.11, as ratios of the A36 target for the 600 gr/ft. LSC.

Table 6.11. Ultimate tensile strength shown as ratios, with the A36 value for the 600 gr/ft. LSC as the denominator

Ultimate Tensile Strength as Ratios					
LSC (gr/ft)	*A36*	*304*	*1018*	*6061*	*4340*
600	1.00	1.54	1.10	0.87	2.71
2,000	1.14	1.50	1.10	0.83	2.71
4,000	1.12	1.54	1.10	0.87	2.71

Figure 6.11 shows the average penetration of the LSC into the targets versus the UTS of the targets. It is important to note that the range of penetration and UTS of 1018 and A36 overlaps in these tests. This was the first analysis that appears to show a correlation between the variable and penetration.
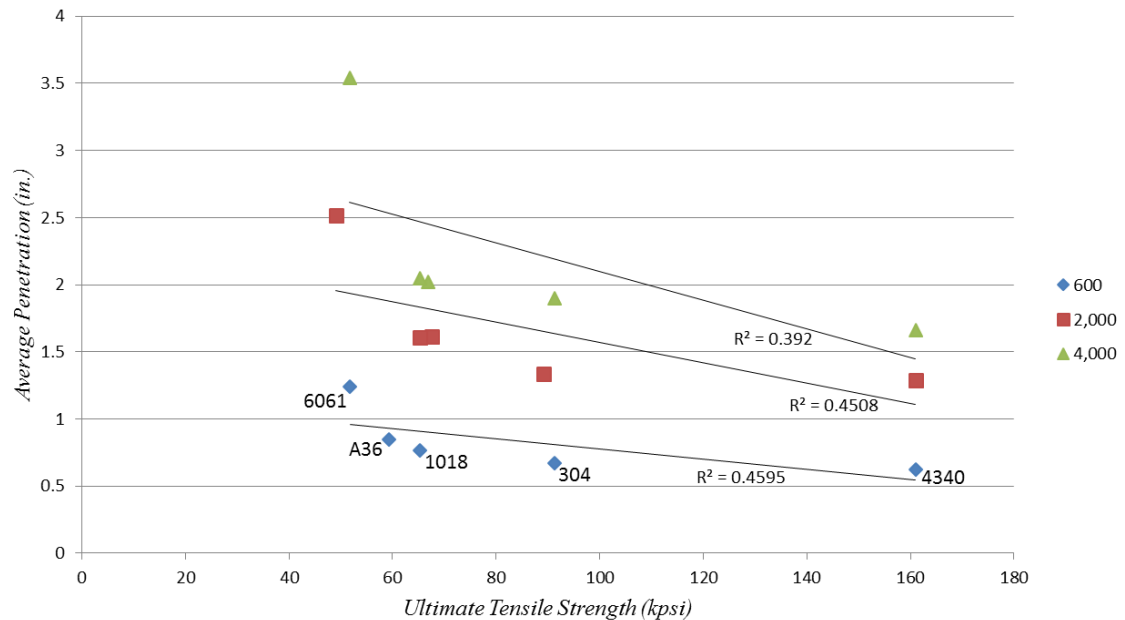
Figure 6.11. Average penetration versus the ultimate tensile strength for the three LSC sizes into the targets

Compared to the graphs showing density and yield strength, it appears that the ultimate tensile strength of a target material is a better indicator of the penetration of an LSC. As the UTS of the target increases, a corresponding decrease in penetration occurs. Unlike the analysis on the effect of yield strength on penetration, the aluminum targets do not appear to be as much of an outlier when examining the effect of tensile strength. The aluminum data points were removed to examine any correlation between the penetration and tensile strength in steels as seen below in Figure 6.12.
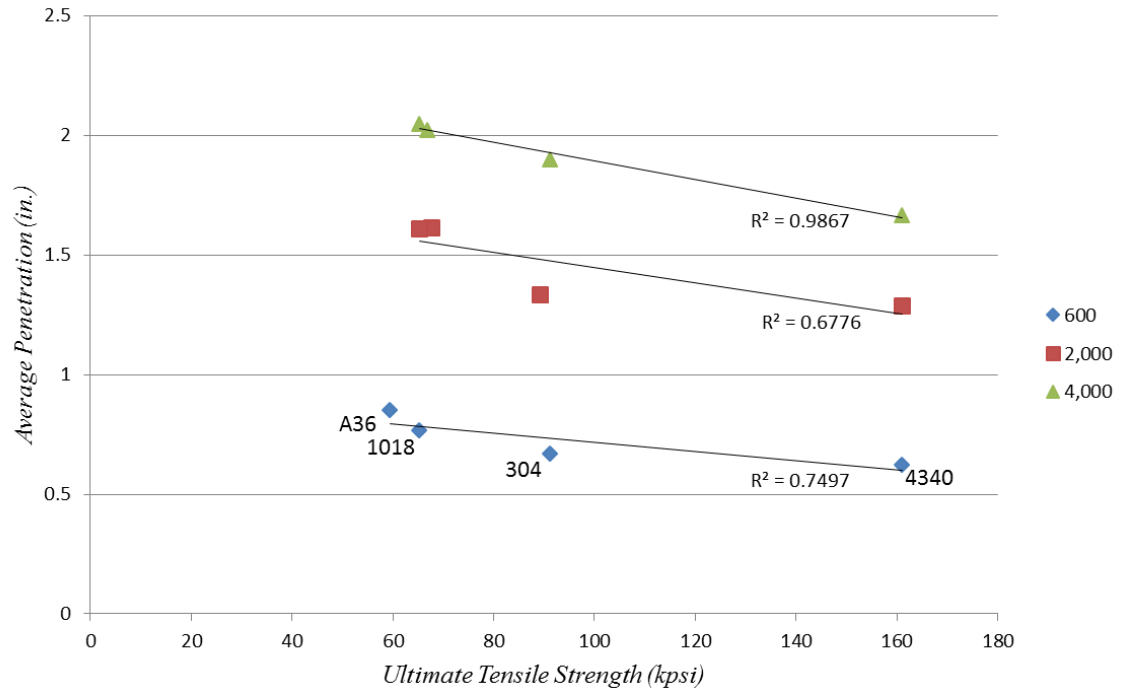
Figure 6.12. Average penetration versus the targets ultimate tensile strength with the aluminum data point removed

A linear regression appears to fit the data better than the previous graphic with the aluminum data point. Future testing with multiple iterations and additional targets with UTS between 100 and 150 ksi will be able to verify any correlation found between the penetration and tensile strength of the target.

6.8. HARDNESS

The hardness of a material is defined as the resistance of a material to a localized deformation, such as denting, scratching, and bending. Testing the hardness of a material is considered a nondestructive test and is easily performed making it a commonly reported quality. The Brinell, Rockwell, Vickers, Mohs, and Knoop hardness tests are all methods

that are used to test a material. The two tests that will be discussed are the Brinell and Rockwell tests.

The Brinell hardness test is a common test used on engineering materials that was invented in 1900. A small, hardened spherical indenter with a known diameter is pressed into the material being tested with a specific force. This will leave a small dent in the material from where the surface area of the indentation can be measured. The load divided by the surface area of the indentation gives the Brinell hardness number (Kalpakjian and Schmid).

The Rockwell hardness test uses a conical indenter rather than the spherical one used in the Brinell test to measure materials hardness. The indenter is pressed into the material with a minor load of 10 kg then, again, with a major load. The major load is removed and held at the minor load. The depth of the indenter can determine the Rockwell hardness at the time of the second minor load. Figure 6.13 helps depict the method of determining the Rockwell hardness (Gordon England).
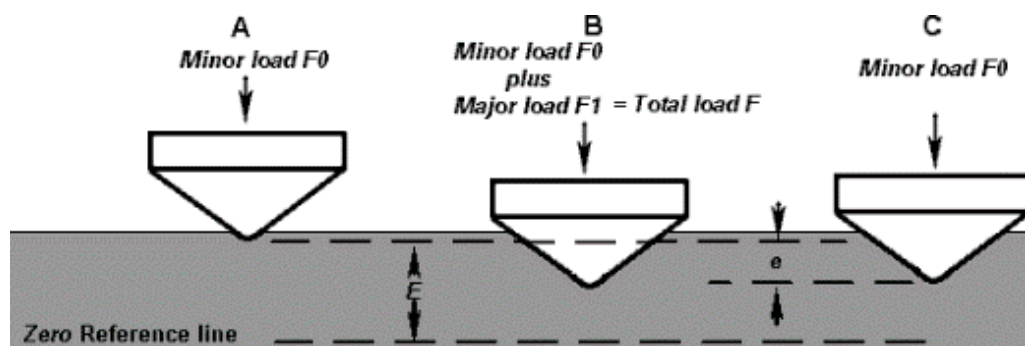
Figure 6.13. Representation of the Rockwell hardness test (Gordon England)

The hardness of different materials are reported within scales that cover a range of hardness levels, typically on the "B" and "C" scale. Typically, the Rockwell hardness

number will be reported as "Hardness Rockwell" followed by the scale used. For example, 100 HRC indicated a hardness of 100 on the C scale.

There is a known linear relationship between hardness, and the ultimate tensile strength of steel. To obtain the Brinell hardness, the PSI must be divided by either 515 or 490, depending on the hardness of the steel (eFunda). Converting between different hardness test numbers is possible and conversion tables are available. Though this is not exact, it is considered close enough for most applications. Figure 6.14 shows the Brinell hardness number that was obtained from converting from the UTS plotted against the penetration values.
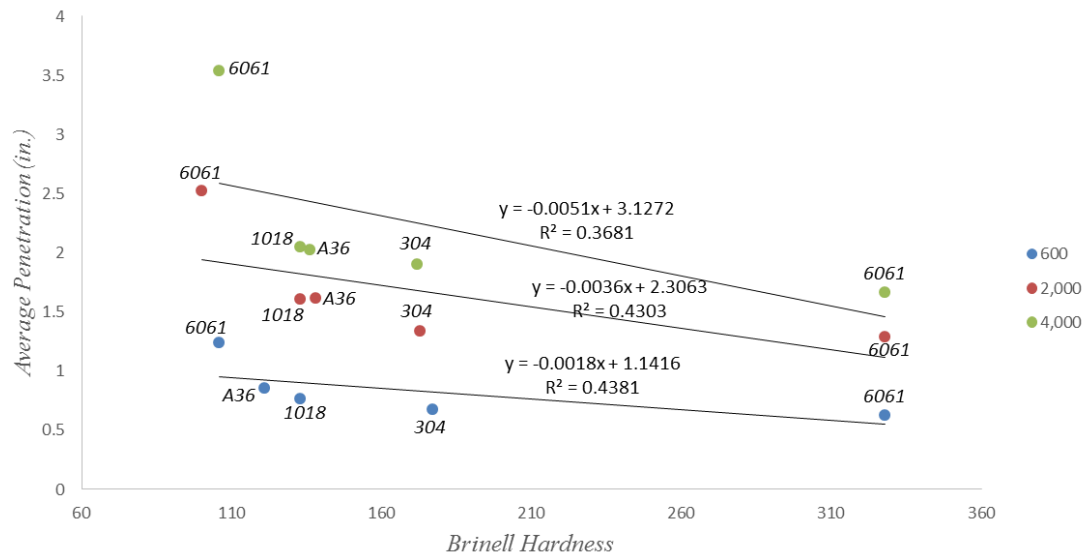
Figure 6.14. Average penetration versus Brinell hardness

As mentioned above, this graph appears to be almost identical to Figure 6.11. Again, more data could possibly strengthen the correlation for this variable since the sample size for each LSC was only five. Removing the aluminum from the plot would result in a cleaner plot similar to the previous analysis.

6.9. POISSON'S RATIO

Each target's Poisson's ratio, ν, was another material property that was examined during this experiment. Poisson's ratio is defined as the ratio of transverse contraction strain to longitudinal strain (strain in the direction of the stretching force) (Greaves, Greer and Lakes). Equations 6 and 7 describe this.

$$\nu = -\varepsilon_{trans}/\varepsilon_{longitudinal} \tag{6}$$

Where the strain, ε, is equal to:

$$\varepsilon = \Delta L/L \tag{7}$$

The Poisson's ratio in each of the target materials is positive, as with most materials because of a materials tendency to become narrower in cross section when they are stretched. A graphical representation of the penetration versus the poisons ratio is shown below in Figure 6.15
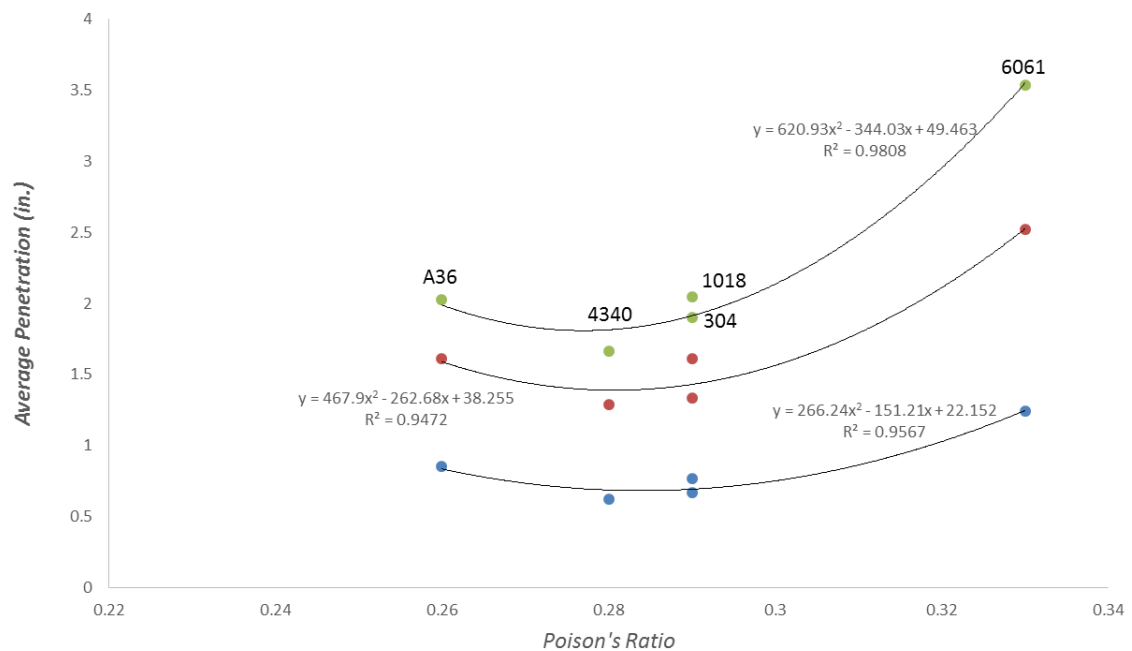
Figure 6.15. Average penetration vs Poisson's ratio for all targets used in this test. Trends are second order polynomials with resulting correlations factors

As seen in the graph, a second order polynomial results in a R^2 value that suggests there is a correlation between the Poisson's ratio and penetration. The reader can see minimums in the fit lines close to a Poisson's ratio of 0.28. This plot suggests that this could be an ideal number for penetration resistance in metal. However, there are only five samples in this analysis and more testing would need to be conducted to better fit predictive curves. Future tests with metal target that have a Poisson's ratio between 0.29 and 0.33 will help fit a predictive curve to this data set. Most metals, however, have a Poisson's ratio of around 0.3. Ceramics have a lower Poisson's ratio while plastics and rubber tend to have a higher Poisson's ratio. More brittle materials will generally have a lower Poisson's ratio while the opposite is true for flexible materials. Poisson's ratio alone will not be able to predict penetration because of the variety of materials that fall within a small range of values. For example, polystyrene foam has a Poisson's ratio that falls within the upper and lower limit of this data set. If one were to use just the analysis on Poisson's ratio, the expected penetration would be about an inch. Common sense tells us otherwise as foam has been used as a standoff for these types of targets with a negligible impact on penetration so this leads to the conclusion that Poisson's ratio alone is not a good predictor. This metric would need to be examined when targets are constrained to a certain strength range, i.e. yield, ultimate tensile.

6.10. BULK, SHEAR, AND YOUNG'S MODULUS

The elastic moduli of these targets are related to each other as well as to the Poisson's ratio. Because the bulk modulus (K), Young's modulus (E), Shear Modulus (G), and Poisson's ratio (v) are all related, an analysis of the moduli is expected to show a

correlation similar to the analysis on Poisson's ratio. These three moduli are all examined to investigate any correlations to penetration.

Figure 6.16 below is a plot of the shear modulus against the average penetration. Which shows correlation factors similar to those seen in the Poisson's ratio plot. A material's shear modulus, or modulus of rigidity, is a ratio of stress to strain when a force is applied to one end of a material while the face parallel and opposite is fixed in place. It is important to note that there is no change in volume during the deformation when testing for this property (Greaves, Greer and Lakes).
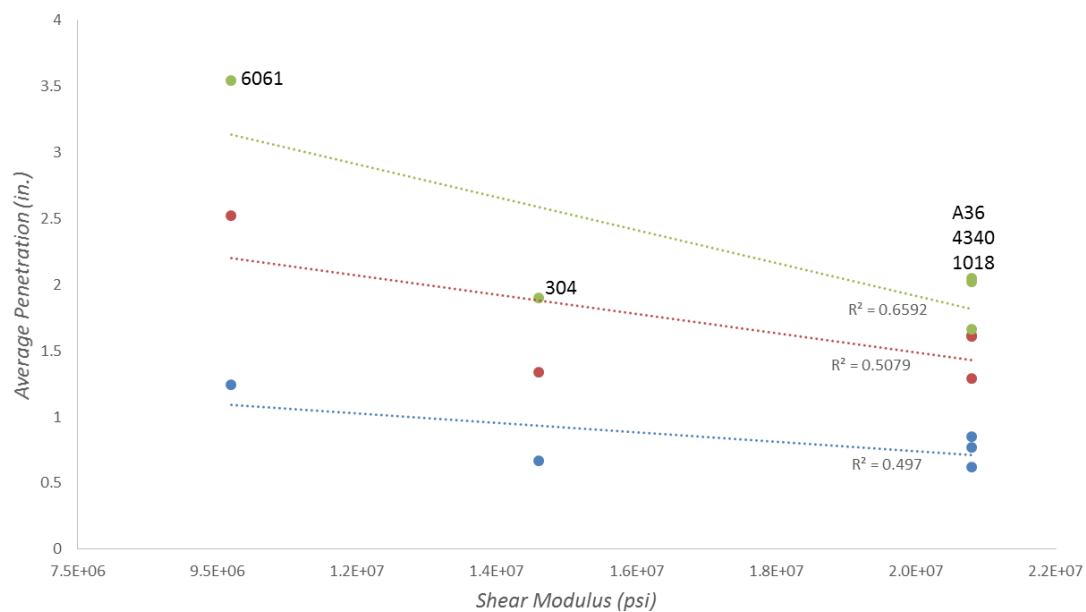
Figure 6.16. Average penetration vs shear modulus. R^2 values are displayed below the best-fit second order polynomials

Figure 6.17 is a graph of the bulk modulus and against the penetration. The bulk modulus of a material is a measure of the materials resistance to a change in volume when under uniform pressurization (Greaves, Greer and Lakes). This is reported in units of pressure, usually pounds per square inch or Pascals. This analysis uses a linear fit line to

show correlation. As with previous analysis, a larger sample size with a range of values would provide a better understanding of how this property contributes to penetration resistance. Figure 6.18 shows the relationship between the targets Young's modulus and the depth of penetration. The Young's modulus, sometimes called tensile or elastic modulus, is a measure of a material's stiffness. The stiffness of a material is the load needed to create a certain deformation (Roylance). The analysis on the correlation between the Young's modulus and the penetration is similar to the other moduli and Poisson's ratio. Using a second order polynomial again, R^2 values are above 87% and suggest that the Young's modulus correlates with the penetration. Again, more testing would be needed to strengthen this correlation. Metals with a Young's modulus between the steel and aluminum would also be beneficial to filling in the gap of missing data.
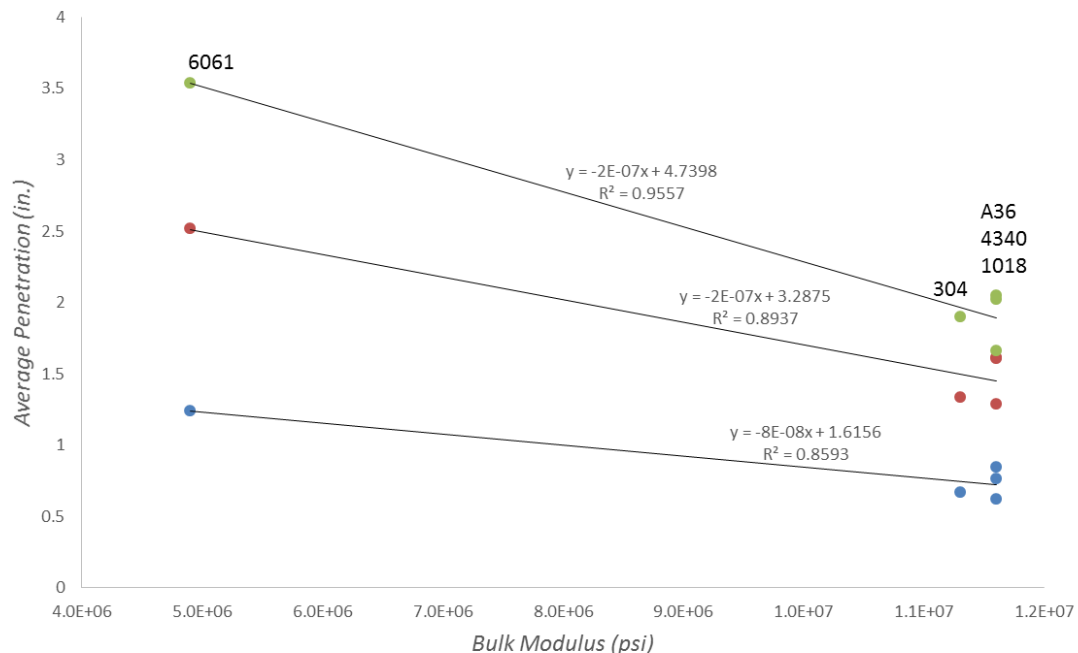
Figure 6.17. Average penetration vs bulk modulus. Three of the five materials are spaced close together on the graph and their position is indicated
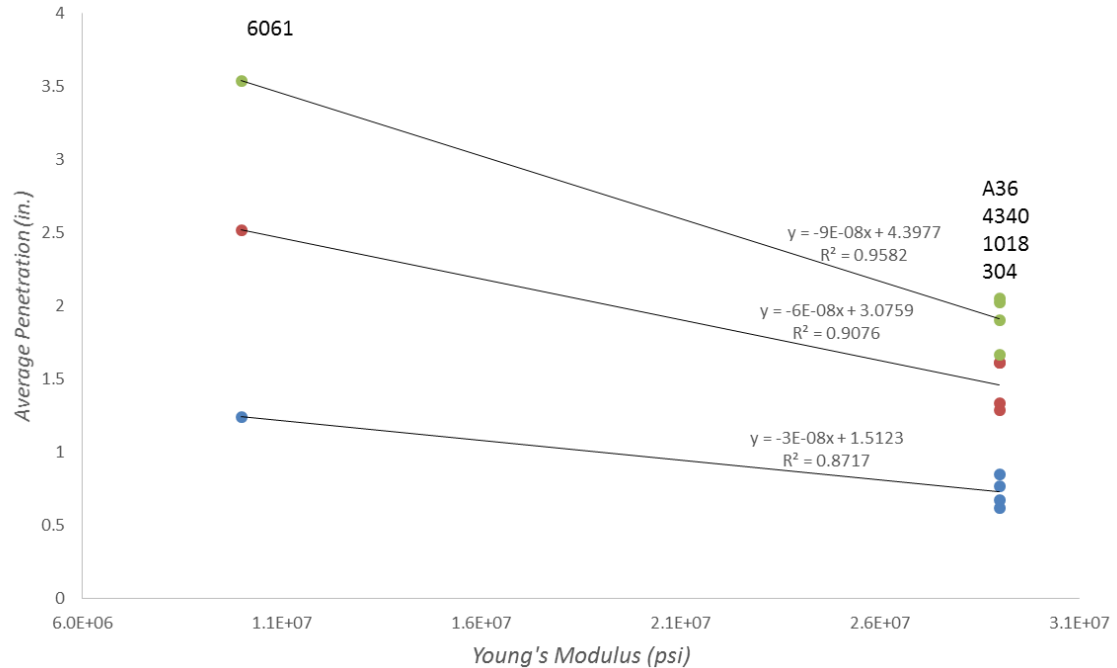
Figure 6.18. Average penetration vs Young's modulus. The steel targets had similar Young's modulus values and appear to be stacked near the right side of the graph

The moduli all have very similar results because of the relationship between them (Greaves, Greer and Lakes). These results show that further tests are needed through a range of Poisson's ratio values. However, these numbers would only make sense when using steel or similar metals for the same reason that Poisson's ratio cannot be used independently to make a prediction on LSC performance.

7. CONCLUSIONS

These tests have shown that there are potential methods of estimating a LSC's penetration into a target. They have also shown that penetration theories developed for CSCs and other projectiles are insufficient to describe penetration of LSCs into metal targets. In equation 3, penetration by a CSC is calculated by using the ratio of jet to target density and the length of the jet. This equation neglects the target materials strength properties. Attempting to estimate LSC performance using equation 3 would result in almost identical predictions for penetration into the steel targets, assuming that the density and length of the copper penetrator remains the same for each size of LSC. Other CSC models, such as equation 4, take into account the target's yield strength in addition to other variables that are all constant in the set of tests for this thesis. It was shown, however, in Figures 6.9 and 6.10 that the yield strength was a poor indicator of performance. The target's tensile strength appeared to be a major factor in the depth of penetration that an LSC could achieve.

This is because the highest tensile strength material tested, 4340 steel, offered the best resistance to penetration when compared to the lower tensile strength materials such as 1018, A36, 4340, and 6061 aluminum. The penetration into aluminum, which had the lowest tensile strength of the tested materials, was between 1.95 and 2.13 times the penetration into 4340 steel. Aluminum experienced between 1.85 and 1.89 times the penetration compared to stainless steel. This agrees with the work done by Smith in 1984 and Vigil & Marchi in 1994 where the penetration into aluminum was roughly twice as much of that into stainless steel. However, these two papers does not attempt to determine

what led to the difference in penetration. Another report (Dehn) shows that penetration of long rods into aluminum was double of that into an unspecified steel.

Equation 3 describes penetration as a function of only the length of the jet and the ratio of jet to target density. This equation has been used to estimate CSC penetration. However, when examining LSC penetration, the equation does not explain the difference between the penetrations found in the four steel targets that all have similar densities. The stainless had the highest density but had less resistance to penetration than 4340 steel, which had a density identical to the other steels used in this test. The limitations of this equation are obvious when looking at the results from Dehn's tests of long rod penetrators into copper. Copper, which has a higher density of any material tested, resisted penetration approximately half as much as the aluminum target. Dehn's tests show that density is not the main property behind penetration resistance for metal targets when discussing long rod penetrators.

The tensile strength of a material appears to be a much better indicator of performance of LSCs into metal targets. The limited sample size did not allow for a stronger correlation between the penetration and tensile strength to be established. The tensile strength appears to be the greatest indicator of penetration resistance and showed a greater correlation than any of the material properties that were reviewed in this thesis. The 4340 steel targets had the highest tensile strength and resisted penetration more than the other materials and targets. The 304 stainless steel targets had the second highest tensile strength and was the second most resistant to penetration.

Another property that did not appear to predict penetration was the yield strength of the target materials. The penetration into 304 and 4340 was similar though the yield

strength of the stainless steel was almost half of that of the 4340 and even lower than the aluminum, which suffered the greatest penetration. The lack of correlation between the target's yield strength and penetration supports the conclusion that a target's yield strength is negligible for copper LSC penetration into metal targets and that the ultimate tensile strength of the target is a much more influential property in resisting penetration.

8. FUTURE WORK

Research on penetration mechanics and theory is a broad topic that has been conducted for a variety of projectiles with various degrees of success. The penetration of LSCs is an area that has a relatively small amount of supporting research compared to its conical counterpart. Therefore, there are many future avenues for research that can benefit and progress the understanding of LSCs.

This research concentrated on the practical aspect of LSC penetration in the five most commonly experienced target materials in LSC use. An important step in research would be validating the results of this experiment with a bigger sample size as well as testing additional target materials and target material properties. Targets with a UTS between 110 and 140 ksi would fill in the "gap" in the data. Expanding this experiment would increase the confidence in the correlation between the material property and penetration while allowing users to choose confidently the LSC to fit their application. The mechanics of the penetrator collapse is one area that has been studied recently, but not fully defined as it is in CSCs. Future researchers would also benefit from being able to characterize the projectile as it relates to the geometry of the charge.

LSCs are typically used in the demolition industry to collapse buildings, bridges, and other structures. Knowing how penetration is effected by the stresses on the target, which would be a structural member, would help users better understand how to use the charges. This means potentially fewer charges and safer demolition of bridges and buildings as the charges will be more effective with optimized placement and charge weight. Additional work should be conducted to define how the size of the target effects the performance of the charge. Understanding how the thickness and width of a target will

affect the penetration by an LSC will allow future researchers to target their research on the material properties instead of any confinement effects.

Further work can also be conducted on the effect of liner material on penetration. This work has been done for long rod penetrators and CSCs but is not very well defined for LSC. The combination of results from this future work would be beneficial for dedicated penetration theories that currently do not exist for LSCs.

APPENDIX A

DATA POINT SETS

Data points for every target are included in the following pages. The tables include forty depth measurements taken at equidistant points along the length of targets. There are three tables, one for each LSC size, showing the penetration for each target material.

600 gr/ft. Target Data. Penetration shown in inches for each target material.

Point	304	6061	4340	A36	1018
1	0.2048	0.528	0.1449	0.1547	0.1673
2	0.3969	0.7631	0.2101	0.3865	0.3211
3	0.4965	0.9843	0.2719	0.6029	0.5183
4	0.6162	1.046	0.4242	0.6712	0.6187
5	0.6533	1.1161	0.5007	0.7297	0.7159
6	0.6354	1.174	0.5336	0.7751	0.7452
7	0.6663	1.2318	0.5384	0.7752	0.755
8	0.672	1.2473	0.5358	0.7945	0.7976
9	0.6574	1.2775	0.572	0.819	0.8294
10	0.6341	1.2775	0.572	0.8143	0.8136
11	0.6947	1.2823	0.599	0.8318	0.8264
12	0.6937	1.3052	0.6003	0.8459	0.8143
13	0.6862	1.3048	0.6227	0.833	0.7955
14	0.7014	1.3057	0.6073	0.8478	0.796
15	0.7006	1.3247	0.6148	0.8792	0.7745
16	0.6939	1.3318	0.6186	0.8986	0.7917
17	0.6869	1.3239	0.6352	0.9296	0.8206
18	0.7069	1.3334	0.6239	0.9117	0.8456
19	0.6962	1.2983	0.6472	0.9279	0.8088
20	0.6823	1.3009	0.6383	0.9102	0.8277
21	0.6782	1.2287	0.6476	0.8713	0.8133
22	0.717	1.2243	0.6461	0.8645	0.8141
23	0.6951	1.2076	0.6437	0.8845	0.8126
24	0.6961	1.2018	0.6584	0.9064	0.8021
25	0.7247	1.2121	0.6552	0.8942	0.7914
26	0.6868	1.2587	0.6154	0.8981	0.8176
27	0.6861	1.2532	0.6021	0.871	0.7672
28	0.6691	1.2409	0.6171	0.8536	0.7701
29	0.6592	1.2409	0.6239	0.8576	0.7823
30	0.6713	1.2409	0.6308	0.8903	0.7554
31	0.6628	1.2427	0.6377	0.858	0.7773
32	0.6529	1.2362	0.6445	0.8586	0.7621
33	0.6463	1.2549	0.6514	0.8348	0.7689
34	0.7056	1.2283	0.6583	0.8534	0.7891
35	0.6762	1.2599	0.6652	0.865	0.7539
36	0.6703	1.2956	0.672	0.8269	0.754
37	0.6222	1.3049	0.6789	0.8119	0.6663
38	0.6048	1.2476	0.6907	0.7855	0.673
39	0.5583	1.0574	0.6202	0.7643	0.6552
40	0.4492	1.0251	0.5356	0.6917	0.6685

2,000 gr/ft. Target Data. Penetration shown in inches for each target material.

Point	304	6061	4340	A36	1018
1	0.4924	1.0204	0.2383	0.5722	0.5791
2	0.6551	1.2294	0.4087	0.7507	0.752
3	0.8291	1.5254	0.5935	0.983	0.8946
4	0.9125	1.7184	0.7264	1.1698	1.0147
5	0.9701	1.8671	0.9053	1.2982	1.1506
6	0.9802	2.0308	0.9975	1.3346	1.2767
7	1.0183	2.0885	1.055	1.3638	1.3435
8	1.071	2.1067	1.1195	1.4193	1.4567
9	1.0638	2.2439	1.1412	1.4659	1.5229
10	1.1104	2.3104	1.2175	1.5432	1.5478
11	1.1745	2.3614	1.3019	1.5793	1.5777
12	1.2173	2.3841	1.3142	1.5741	1.6086
13	1.2393	2.3854	1.343	1.5874	1.6537
14	1.1951	2.403	1.3874	1.5695	1.6536
15	1.2046	2.5705	1.388	1.6111	1.6486
16	1.2251	2.5149	1.3311	1.6236	1.645
17	1.2942	2.5028	1.3343	1.6299	1.6253
18	1.301	2.3895	1.3349	1.6387	1.6042
19	1.2822	2.4856	1.3518	1.6827	1.595
20	1.2645	2.4862	1.3499	1.7062	1.6038
21	1.3269	2.5269	1.3342	1.6802	1.6412
22	1.3831	2.4892	1.3542	1.6756	1.6738
23	1.3891	2.5613	1.3476	1.6763	1.6271
24	1.3716	2.6069	1.3352	1.6818	1.6455
25	1.3553	2.6324	1.3378	1.6994	1.6457
26	1.3624	2.6174	1.3214	1.7326	1.6637
27	1.4148	2.5648	1.2731	1.7161	1.6291
28	1.4469	2.5382	1.2701	1.753	1.6431
29	1.4508	2.5652	1.2693	1.7266	1.704
30	1.4508	2.6021	1.2901	1.7431	1.725
31	1.437	2.5904	1.284	1.6978	1.7258
32	1.4322	2.5333	1.3383	1.69	1.7217
33	1.4463	2.5852	1.3706	1.6606	1.6655
34	1.4555	2.6179	1.3219	1.6461	1.6557
35	1.4523	2.6204	1.3167	1.6187	1.6577
36	1.4491	2.5677	1.3185	1.5935	1.659
37	1.4458	2.4312	1.3077	1.5567	1.5775
38	1.3341	2.3832	1.3048	1.568	1.557
39	1.2591	2.4673	1.2857	1.5479	1.529
40	1.2049	2.4049	1.1555	1.4806	1.4859

4,000 gr/ft. Target Data. Penetration shown in inches for each target material.

Point	304	6061	4340	A36	1018
1	0.4876	1.6309	0.6448	0.5553	0.5717
2	0.7098	1.7794	0.7201	0.8564	0.7208
3	0.8525	2.182	0.8787	1.1128	1.0165
4	0.9789	2.3673	0.9446	1.2497	1.1494
5	1.1091	2.6111	1.1542	1.3735	1.2748
6	1.3111	2.7995	1.3588	1.6285	1.4992
7	1.465	2.9928	1.3899	1.6797	1.7474
8	1.5861	3.1459	1.5398	1.7648	1.8708
9	1.6409	3.2693	1.5281	1.8399	1.8708
10	1.723	3.2973	1.5848	1.9293	1.8969
11	1.8183	3.3253	1.6331	1.8712	1.9072
12	1.9065	3.4068	1.6779	1.9358	1.8984
13	1.9156	3.4908	1.5803	1.8998	1.9746
14	1.8924	3.5473	1.5966	1.9143	2.0739
15	1.83	3.6048	1.6506	2.0524	2.1147
16	1.8574	3.6719	1.6057	2.0326	2.1026
17	1.8655	3.7034	1.6297	1.9647	2.0889
18	1.8739	3.6603	1.6198	1.9688	2.063
19	1.865	3.6075	1.7038	1.9633	2.0368
20	1.8401	3.5562	1.6806	2.0395	2.0733
21	1.8664	3.5513	1.6553	2.0544	2.0751
22	1.8815	3.5656	1.6653	2.0187	2.0521
23	1.8972	3.5714	1.7253	2.0047	2.0862
24	1.8834	3.5894	1.6873	2.0339	2.123
25	1.9083	3.6115	1.6863	2.042	2.1094
26	1.945	3.704	1.7231	2.0955	2.1316
27	1.9701	3.699	1.7429	2.0982	2.0848
28	1.9767	3.6945	1.7362	2.1095	2.1334
29	1.9794	3.7184	1.7428	2.0571	2.1271
30	1.9908	3.7206	1.7258	2.009	2.1646
31	2.0274	3.6904	1.7354	2.032	2.1405
32	2.028	3.6601	1.7826	2.1273	2.1194
33	1.9711	3.6665	1.7837	2.1016	2.0705
34	1.945	3.7037	1.7338	2.0053	2.0986
35	1.9344	3.7046	1.7169	1.997	2.0304
36	1.9591	3.7228	1.8285	1.9921	2.0568
37	1.9661	3.7808	1.7815	2.1229	2.0888
38	1.9757	3.7793	1.7023	2.1768	2.1266
39	1.9851	3.7505	1.7225	2.0599	2.1182
40	1.9458	3.6491	1.7545	2.0478	2.0797

APPENDIX B
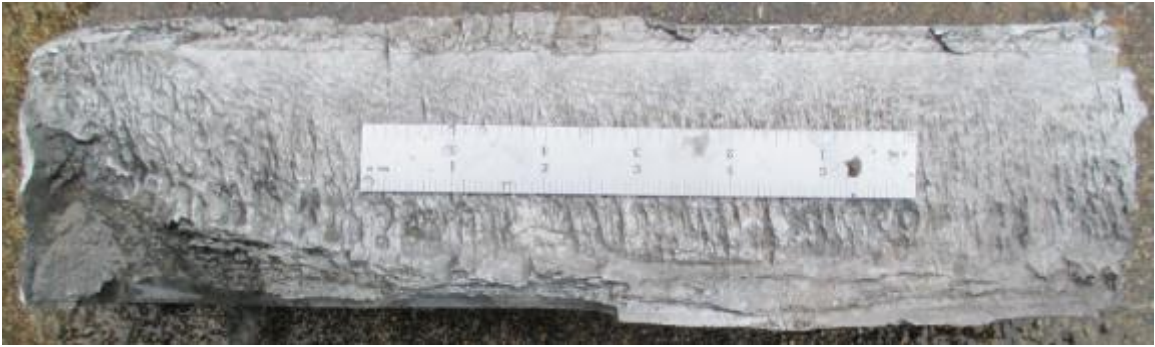
PHOTOGRAPHS OF 304 TARGETS

Photographs of the 304L stainless steel targets. The first image is the 600 gr/ft. target.
The next two are the 4,000 gr/ft. targets. The 304 targets did not fracture when testing so
the author cut these in half in order to look at the penetration depth. Most of these targets
were destroyed during the cutting process.
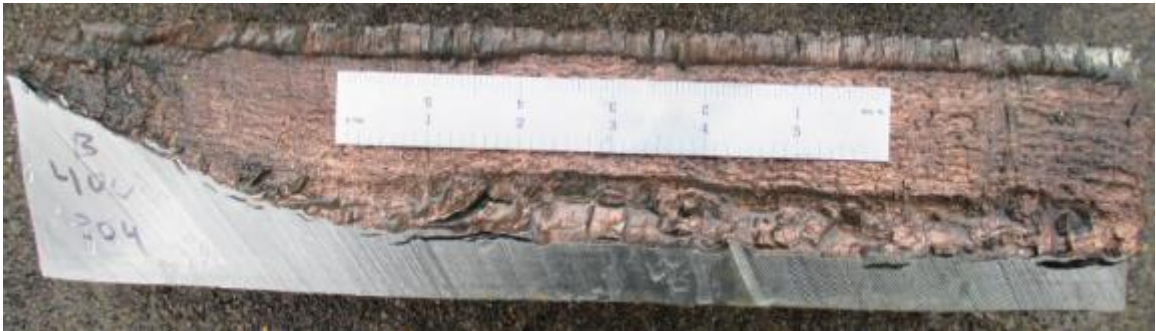
APPENDIX C

PHOTOGRAPHS OF 6061 TARGETS

The following images are of the 6061-T6 aluminum targets. The 600 gr/ft. targets were destroyed during data collection. The first image is a 2,000 gr/ft. target. The next two are targets from the 4,000 gr/ft. test. The last image is a target from an early test where penetration was through the target, which prompted thicker aluminum targets.
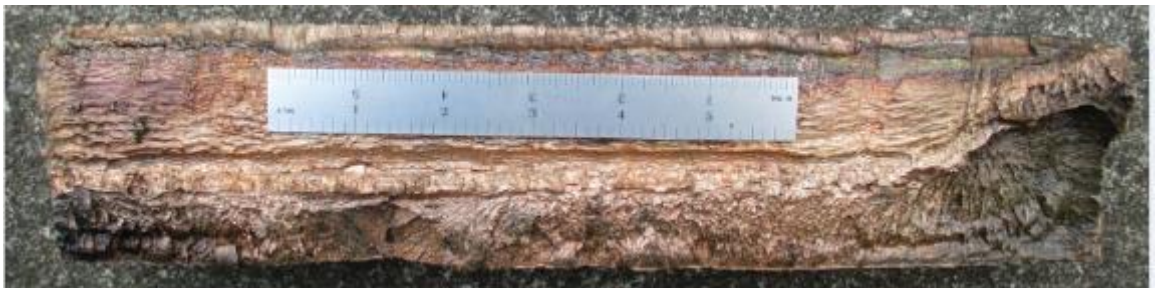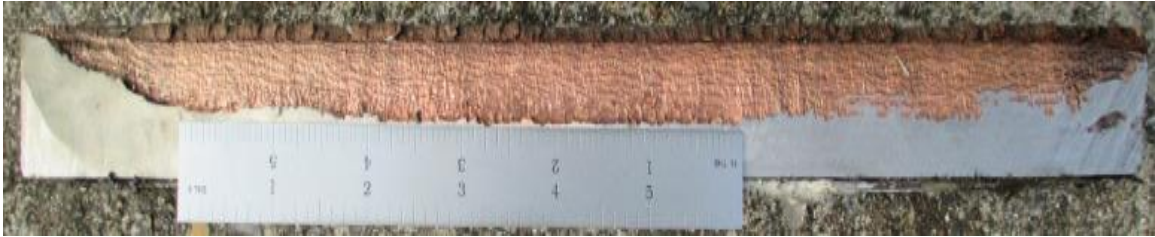
APPENDIX D

PHOTOGRAPHS OF 4340 TARGETS

Two out of three 4340 steel targets fractured during testing. The author needed to cut the 600 gr/ft. target post-test and half of this target was damaged and not photographed. From top to bottom, the following page contains images for one-half of the 600 gr/ft. target, both halves of the 2,000 gr/ft. target, and both halves of the 4,000 gr/ft. target.
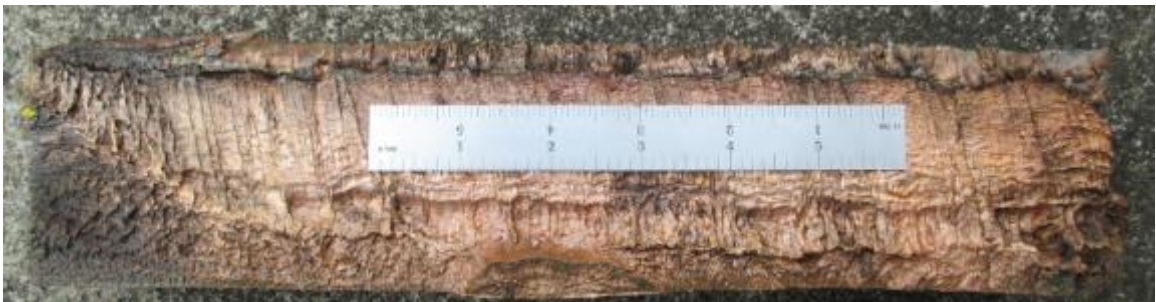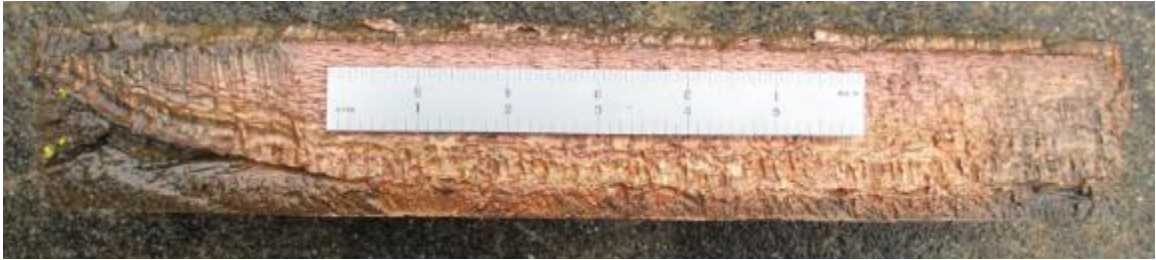
APPENDIX E

PHOTOGRAPHS OF 4340 TARGETS

The author had to cut the A36 target for the 600 gr/ft. tests post-test to collect penetration data. This resulted in half of the target destroyed. The remaining half of this target, as well as both halves of the other targets are shown on the following page. From top to bottom, these pictures show the 600 gr/ft. to the 4,000 gr/ft. targets.

APPENDIX F

PHOTOGRAPHS OF 1018 TARGETS

All 1018 steel targets fractured during the test. The images in this appendix show both halves of each target, starting with the 600 gr/ft. target on top and ending with the 4,000 gr/ft. target.

BIBLIOGRAPHY

ASTM International. *ASTM A1018 / A1018M-15 Standard Specification for Steel, Sheet and Strip, Heavy-Thickness Coils, Hot-Rolled, Carbon, Commercial, Drawing, Structural, High-Strength Low-Alloy, High-Strength Low-Alloy with Improved Formability, and Ultra-High Strength*. West Conshohocken, 2012.

—. *ASTM A249/A249M-14a Standard Specification for welded Austententic Steel Boiler, Superheater, Heat-Exchanger, and Condenser Tubes*. West Conshohocken, 2015.

—. *ASTM A36 / A36M - 14 Standard Specification for Carbon Structural Steel*. West Conshohocken, 2014.

—. *ASTM A829/A829M-14 Standard Specification for Alloy Structural Steel Plates*. West Conshohocken, 2015.

—. *ASTM B221-12 Standard Specification for Aluminum and Aluminum-Alloy Extruded Bars, Rods, Wire, Profiles, and Tubes*. West Conshohocken, 2012.

Brammfitt, Bruce L and Arlan O Benscoter. *Metallographer's Guide: Practices and Procedures for Irons and Steels*. Materials Park: ASM International , 2002.

Burch, Brian T. *Determining and Mitigating the Effects of Firing a Linear Shaped Charge Underwater*. Thesis. Rolla: Missouri University of Science and Technology, 2014.

Cooper, Paul W. *Explosives Engineering*. Hoboken: Wiley-VCH, 1996.

Dehn, James T. *Technical Report BRL-TR-2770: A Unified Theory of Penetration (U)*. Ballistic Research Laboratory. Aberdeen Proving Ground, 1986.

Dossett, Jon L and Howard E Boyer. *Practical Heat Treating*. Materials Park: ASM International, 2006.

eFunda. "Convert Hardness." 2015. 18 November 2015. <http://www.efunda.com/units/hardness/convert_hardness.cfm?cat=Steel&HD=Approx.%20TS>.

Goodfellow. *Stainless Steel - Grade 304*. n.d. 19 June 2014. <http://www.azom.com/article.aspx?ArticleID=965>.

Gordon England. *Rockwell Hardness Test*. n.d. 24 June 2014. <http://www.gordonengland.co.uk/hardness/rockwell.htm>.

Greaves, G N, et al. "Poisson's Ratio and Modern Material." *Nature Materials* 10 (2011): 823-837.

Hussain, G, et al. "Experimental and Simulation Optimization Analysis of the Whipple Shields Against Shaped Charge." *Acta Mechanica Sinica* 28.3 (2012): 877-884.

Johnston, Matthew and Seokbin Lim. "Numerical Observation of the Jet Flight Patterns of Linear Shaped Charges." *Applied Sciences* 2.3 (2012): 629-640.

Kalia, Hemendra Nath. *Penetration in Granite by Shaped Charge Liners of Various Metals*. Doctoral Dissertations. Rolla, 1970.

Kalpakjian, Serope and Steven Schmid. *Manufacturing, Engineering, & Technology*. Prentice Hall, 2006.

Kennedy, Donald R. *History of the Shaped Charge Effect: The First 100 Years*. Mountain View: D.R. Kennedy & Associates, Inc, 1983.

Lim, Seokbin. *An Investigation of the Characteristics of Linear Shaped Charges used in Demolition*. Thesis. Rolla: Missouri S&T, 2003.

MatWeb. *AISI 1018 Steel*. 2014. 17 June 2014. <http://www.matweb.com/search/datasheet.aspx?matguid=3f2ce033f2fc4bc0b0165cc0bd044b4d>.

—. "AISI 4340 Steel." n.d. 11 November 2015. <http://asm.matweb.com/search/SpecificMaterial.asp?bassnum=M434AE>.

Novokshanov, Roman and John Ockendon. "Elastic-plastic Modelling of Shaped Charge Jet Penetration." *Proceedings of the Royal Society A* 462.2076 (2006): 3663-3681.

O'Neal Steel. *A1018 Plate*. n.d. 17 June 2014. <http://www.onealsteel.com/carbon-steel-plate-a1018.html>.

Ortel, Matthew. *A Modified Initiation and Cut Profile Study of the 10500 Grain Per Foot Linear Shaped Charge*. Thesis. Rolla: Missouri University of Science and Technology, 2014.

Pazienza, G. *Steel Cutting Using Linear-Shaped Charges*. Luxembourg: Office for Official Publications of the European Commision, 1995.

Phelps, Kevin L., D Nolan and Jason Baird. "New Methodology in Measuring Experimental Results of Linear Shaped Charges Using Digital Software." *Proceeding of the Thirty-Ninth Annual Conference of Explosive and Blasting Technique*. Dallas, 2013.

Poole, Chris. *Penetration of a Shaped Charge*. Corpus Christi College. Oxford, 2005.

Raymond, C F. *Definition of a Continuum*. n.d. 18 April 2015. <http://earthweb.ess.washington.edu//Glaciology/courses/ess511/cfr_ch1.pdf>.

Roylance, David. *Mechanical Properties of Materials*. New York: John Wiley, 1995.

Sanders, Robert E. "Technology Innovation in Aluminum Products." *The Journal of the Mineral, Metals, and Materials Society* 53.2 (2001): 21-25.

Smart, Michael and Arnold Steber. "Hull Maintenance Technician." 1995.

Smith, James Lee. "Pyrotechnic Shock: A Literature Survey of the Linear Shaped Charge (LSC)." National Aeronautics and Space Administration, May 1984.

U.S. Department of Energy. "DOE Fundamentals Handbook: Material Science." 1993. Handbook.

U.S. Department of Transportation: Federal Aviation Administration. *Aviation Maintenance Technician Handbook*. Oklahoma City: U.S. Department of Transportation, Federal Aviation Administration, Airmen Testing Standards Branch, 2008. Handbook.

Vigil, Manuel G and Donald L Marchi. "Annular Precision Linear Shaped Charge Flight Termination System for the ODES Program." Albuquerque: Sandia National Labroratories, June 1994.

Walters, William. *ARL-SR-150: Introduction to Shaped Charges*. Aberdeen Proving Grounds: Army Research Laboratory, 2007.

VITA

Kevin L. Phelps graduated from Rolla High School in 2008. He received his B.S. in Mining Engineering from the Missouri University of Science and Technology in December 2014 and a Master of Science in Explosives Engineering at Missouri S&T in May 2016.